CMS-SUS-20-002

arXiv:2107.10892v2 [hep-ex] 9 Nov 2021

Combined searches for the production of supersymmetric top quark partners in proton-proton collisions at $\sqrt{s} = 13\,\text{TeV}$

The CMS Collaboration*

Abstract

A combination of searches for top squark pair production using proton-proton collision data at a center-of-mass energy of 13 TeV at the CERN LHC, corresponding to an integrated luminosity of $137\,\text{fb}^{-1}$ collected by the CMS experiment, is presented. Signatures with at least 2 jets and large missing transverse momentum are categorized into events with 0, 1, or 2 leptons. New results for regions of parameter space where the kinematical properties of top squark pair production and top quark pair production are very similar are presented. Depending on the model, the combined result excludes a top squark mass up to 1325 GeV for a massless neutralino, and a neutralino mass up to 700 GeV for a top squark mass of 1150 GeV. Top squarks with masses from 145 to 295 GeV, for neutralino masses from 0 to 100 GeV, with a mass difference between the top squark and the neutralino in a window of 30 GeV around the mass of the top quark, are excluded for the first time with CMS data. The results of theses searches are also interpreted in an alternative signal model of dark matter production via a spin-0 mediator in association with a top quark pair. Upper limits are set on the cross section for mediator particle masses of up to 420 GeV.

*See Appendix A for the list of collaboration members

1 Introduction

The standard model (SM) of particle physics describes subatomic phenomena with outstanding precision. However, the SM cannot address several open questions such as the hierarchy problem [1, 2] and the absence of a suitable particle candidate for dark matter (DM) [3, 4]. Supersymmetry (SUSY) [5–12] is a well-known extension of the SM that can resolve both of these problems by introducing a relation between bosons and fermions. For each known particle, it assigns a new SUSY partner that differs by a half unit of spin. SUSY provides a natural solution to the gauge hierarchy problem provided that the SUSY partners of the top quark, gluon, and Higgs boson are not too massive. While difficult to quantify precisely, values of the top squark mass up to the 1 TeV range are favored [1, 13–15]. The lightest SUSY particle (LSP), which is potentially massive, may be a viable DM candidate if it is stable and electrically neutral.

This paper presents the combination of previously published searches [16–18] for the pair production of SUSY top quark partners in final states without leptons, with one, or with two charged leptons, in events from proton-proton (pp) collisions at a center-of-mass energy ($\sqrt{s}$) of 13 TeV at the CERN LHC, corresponding to an integrated luminosity of 137 fb^{-1}, and referred to here as inclusive analyses. It also includes a new analysis targeting a parameter space where the mass difference between the top squark and the neutralino is close to the top quark mass, whose results are combined with the previously published studies. All analyses are performed with the data set collected in 2016–2018 (Run 2) by CMS.

The inclusive searches are interpreted in terms of top squark pair production with two different subsequent decays, as described in the simplified model context [19–21]. Two decay chains are considered, both of which lead to a signature with a neutralino ($\widetilde{\chi}_1^0$), which is the LSP, a W boson and a bottom quark. These are the direct decay of the top squark to a top quark and a neutralino, and the decay of the top squark to a chargino ($\widetilde{\chi}_1^\pm$) and a bottom quark where the chargino decays to a W boson and a neutralino. Three simplified models are used for interpretation. In the first model, both top squarks decay according to the first decay chain; in the second model, both decay according to the second decay chain; in the third model, these two decays occur with equal probability. The mass of the chargino in the second model is chosen to be an arithmetic average of the top squark mass ($m_{\widetilde{t}_1}$) and the LSP mass ($m_{\widetilde{\chi}_1^0}$), while in the third model the mass splitting between the neutralino and chargino is assumed to be 5 GeV. Typical diagrams are shown in Fig. 1. In previous analyses by the CMS collaboration top squark masses up to 1310 GeV have been excluded [16–18, 22–29]. Limits on the production of top squark pairs with masses up to 1260 GeV have been set by the ATLAS Collaboration [30–35].
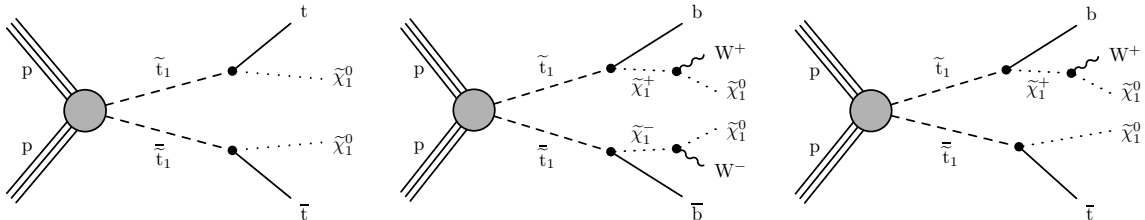

Figure 1: Diagrams of top squark pair production with further decay of each top squark into a top quark and a neutralino (left), of each top squark into a chargino and a neutralino, with the chargino decaying then into a bottom quark and a W boson (center), and with a combination of the two top squark decay scenarios (right).

If the mass difference between the top squark and the lightest neutralino in the $\widetilde{t}_1 \to t\widetilde{\chi}_1^0$ model

is close to the mass of the top quark (m_t), the kinematic distributions of the final states of the SUSY signal are very similar to those of SM top quark pair ($\text{t}\bar{\text{t}}$) production processes. Therefore, this is a difficult region in which to search for a signal. In this case, the signal acceptance strongly depends on $m_{\tilde{\text{t}}_1}$ and $m_{\tilde{\chi}_1^0}$. The boundaries of the corridor are taken to be $\Delta m_\text{cor} = 30\,\text{GeV}$ and $m_{\tilde{\text{t}}_1} \lesssim 275\,\text{GeV}$, where $\Delta m_\text{cor} \equiv |\Delta m\,(\tilde{\text{t}}_1, \tilde{\chi}_1^0) - 175\,\text{GeV}|$ and 175 GeV is the reference value of the top quark mass. The top quark corridor was not included in the parameter space addressed by the previous inclusive searches by the CMS Collaboration [16–18, 22–29].

In the top quark corridor region, the signal could be observed as an excess over the $\text{t}\bar{\text{t}}$ background prediction [36], but the sensitivity to $m_{\tilde{\chi}_1^0} \geq 20\,\text{GeV}$ is limited. A dedicated search was performed with the data set collected in 2016 by CMS [37], that excluded the presence of top squark production up to $m_{\tilde{\text{t}}_1} = 240\,\text{GeV}$ for $\Delta m_\text{cor} = 0$ and up to about $m_{\tilde{\text{t}}_1} = 208\,\text{GeV}$ for $\Delta m_\text{cor} = 7.5\,\text{GeV}$ at 95% confidence level. An analysis of the top quark corridor by the ATLAS Collaboration has set exclusion limits for top squark masses between 170 and 230 GeV [38].

This paper presents a new dedicated search in events with an opposite-charge lepton pair that is sensitive to the top quark corridor region. The sensitivity in the top quark corridor is extended by using a larger data set and a more sophisticated strategy, using a deep neural network (DNN) [39] to exploit the differences between the signal and the SM $\text{t}\bar{\text{t}}$ production, which is the main background.

In order to reduce the background from $\text{t}\bar{\text{t}}$ events, the missing transverse momentum ($\vec{p}_\text{T}^{\,\text{miss}}$) is used together with the so-called "stransverse" mass of the leptons ($m_{\text{T2}}(\ell\ell)$) [40], defined as

$$m_{\text{T2}}(\ell\ell) = \min_{\vec{p}_{\text{T1}}^{\,\text{miss}}+\vec{p}_{\text{T2}}^{\,\text{miss}}=\vec{p}_\text{T}^{\,\text{miss}}} \left(\max\left[m_\text{T}(p_\text{T}^{\ell 1}, \vec{p}_{\text{T1}}^{\,\text{miss}}), m_\text{T}(p_\text{T}^{\ell 2}, \vec{p}_{\text{T2}}^{\,\text{miss}}) \right] \right),$$

where ℓ refers to an electron or a muon, m_T is the transverse mass, and $\vec{p}_{\text{T1}}^{\,\text{miss}}$ and $\vec{p}_{\text{T2}}^{\,\text{miss}}$ correspond to the estimated transverse momenta of the two invisible particles (neutrinos in the case of $\text{t}\bar{\text{t}}$ events) that are presumed to determine the total $\vec{p}_\text{T}^{\,\text{miss}}$ of an SM event. The transverse mass is calculated for each lepton-neutrino pair, for different assumptions of the neutrino transverse momentum ($\vec{p}_{\text{T}i}^{\,\text{miss}}$). The computation of $m_{\text{T2}}(\ell\ell)$ is done using the algorithm discussed in Ref. [41]. A signal region is defined applying requirements on $m_{\text{T2}}(\ell\ell)$ and on p_T^miss, the magnitude of $\vec{p}_\text{T}^{\,\text{miss}}$. A DNN is used to optimize the sensitivity for signal at each mass point.

We also consider the alternative model $\text{t}\bar{\text{t}} + \text{DM}$ shown in Fig. 2, in which a DM particle is produced in association with a pair of top quarks. In this simplified model, a scalar (ϕ) or pseudoscalar (a) particle mediates the interaction between SM quarks and a new Dirac fermion (χ), which is the DM candidate particle [42–46]. Under the assumption of minimal flavor violation [47, 48] the spin-0 mediators couple to quarks having mass m_q with SM-like Yukawa couplings proportional to $g_\text{q} m_\text{q}$, where the coupling strength g_q is taken to be 1. The coupling strength g_DM of the mediator to the DM particles is also set to 1. In the case of a scalar mediator, mixing with the SM Higgs boson is neglected. Prior searches by the ATLAS and CMS Collaborations excluded scalar and pseudoscalar mediator particles with a mass of up to 290 and 300 GeV, respectively [30, 49–52].

2 The CMS detector

The central feature of the CMS apparatus is a superconducting solenoid of 6 m internal diameter, providing a magnetic field of 3.8 T. Within the solenoid volume are a silicon pixel and strip
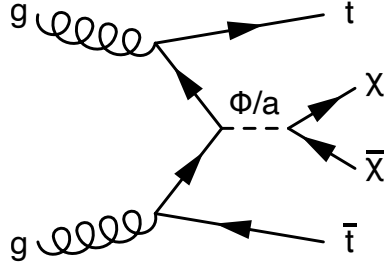
Figure 2: Feynman diagram of direct DM production through a scalar (*φ*) or pseudoscalar (a) mediator particle, in association with a top quark pair.

tracker, a lead tungstate crystal electromagnetic calorimeter (ECAL), and a brass and scintillator hadron calorimeter (HCAL), each composed of a barrel and two endcap sections. Forward calorimeters extend the pseudorapidity coverage provided by the barrel and endcap detectors. Muons are detected in gas-ionization chambers embedded in the steel flux-return yoke outside the solenoid.

Events of interest are selected using a two-tiered trigger system. The first level, composed of custom hardware processors, uses information from the calorimeters and muon detectors to select events at a rate of around 100 kHz within a fixed latency of about 4 μs [53]. The second level, known as the high-level trigger, consists of a farm of processors running a version of the full event reconstruction software optimized for fast processing, and reduces the event rate to around 1 kHz before data storage [54].

A more detailed description of the CMS detector, together with a definition of the coordinate system used and the relevant kinematic variables, can be found in Ref. [55].

3   Monte Carlo simulation

Monte Carlo (MC) simulation is used to design the searches, predict or aid the prediction of the background events from SM processes, and to provide estimations of the expected SUSY and $t\bar{t} + DM$ signal event yields.

Several models from the simplified model spectra [19, 21] are used to simulate the SUSY signals. The helicity states of the produced top quarks are not considered in these models, and in the simulation the top quarks are treated as unpolarized. The generation of signal samples is performed using the MADGRAPH5_aMC@NLO generator (MADGRAPH) [56, 57] (version 2.2.2 for 2016 and version 2.4.2 for 2017 and 2018) at leading order (LO) in quantum chromodynamics (QCD) with up to two additional partons from initial-state radiation (ISR). To improve on the MADGRAPH modeling of the multiplicity of additional jets from ISR, MADGRAPH signal events are reweighted based on the number of ISR jets (N_J^{ISR}). These weights are obtained using a $t\bar{t}$ MADGRAPH MC sample, so as to make the $t\bar{t}$ jet multiplicity agree with data. The reweighting factors vary between 0.92 and 0.51 for N_J^{ISR} between 1 and 6, respectively.

Signal samples of the $t\bar{t} + DM$ model [58] are generated using MADGRAPH v2.4.2 at LO with at most one additional parton in the matrix element calculations. Samples for mediator masses of 50, 100, 200, 300, and 500 GeV have been generated for both the scalar and pseudoscalar models. The mass of the DM particle is set to 1 GeV while a value of 1 is chosen for the couplings.

The SM $t\bar{t}$ process is simulated using the POWHEG (v2) [59–61] generator at next-to-leading order (NLO) for the dilepton analyses or the MADGRAPH generator at LO for the analyses of

zero or one lepton events. In the top quark corridor analysis the POWHEG generator is used, as this analysis relies on a precise estimate of the $t\bar{t}$ background and its associated modeling uncertainties, which are better described in CMS by the POWHEG generator [36, 62]. This sample is also used to calculate the dependence of the $t\bar{t}$ acceptance on m_t and on the factorization and renormalization scales (μ_F, μ_R, respectively). A parameter denoted as h_{damp} is used in the modeling of the parton shower matrix element [63, 64]. The central value and uncertainties in h_{damp} are discussed in Section 6.4.2.

The POWHEG v1 [65] generator is used for the single top quark and antiquark production in association with a W boson (tW) at NLO. The MADGRAPH v2.2.2 [56] generator is used at NLO for modeling the Drell–Yan (DY) process, the production of W or Z bosons in association with $t\bar{t}$ events ($t\bar{t}$W, $t\bar{t}$Z), and the WW, WZ, and ZZ production processes. The production of the DY process is simulated with up to two additional partons [66], and the FxFx scheme is used for the matching of jets from the matrix element calculations and from parton showers. Samples of W+jets, Z+jets events (with $Z \rightarrow \nu\bar{\nu}$), γ+jets, and QCD multijet production are simulated with up to four extra partons in the matrix element calculations using the MADGRAPH (v2.2.2 in 2016 and v2.4.2 in 2017 and 2018) event generator at LO. Double counting of the partons generated with MADGRAPH and via the parton shower is removed using the MLM [57] matching scheme.

The NNPDF 3.0 [67] parton distribution function (PDF) set is used for generating the samples corresponding to the 2016 period, while the NNPDF 3.1 NNLO [68] PDF is used for the 2017 and 2018 samples. Parton showering and hadronization are handled by PYTHIA v8.226 (8.230) [69, 70] using the underlying event tune CUETP8M2T4 [63] for SM $t\bar{t}$ events for the 2016 (2017, 2018) period, the CUETP8M1 [71] tune for all other background and signal events in the 2016 period, and the CP5 tune [64] for all background and signal events of the 2017 and 2018 periods. The nominal top quark mass is 172.5 GeV in all the samples.

The GEANT4 package [72] is used to simulate the CMS detector for samples of the SM processes, the $t\bar{t}$ + DM signal processes, and SUSY signal samples where $m_{\tilde{t}_1} - m_{\tilde{\chi}_1^0}$ is close to the top quark mass. The CMS fast simulation program [73, 74] is used to simulate the detector response for the remaining signal samples. The effect of additional interactions in the same event (referred to as pileup) is accounted for by simulating additional minimum bias interactions for each hard scattering event. The observed distribution of the number of pileup interactions, which has an average of 23 and 32 collisions per bunch crossing for the 2016 period, and for the 2017 and 2018 periods, respectively, is reproduced by the simulation.

Simulated background events are normalized according to the integrated luminosity and the theoretical cross section of each process. The latter are computed at next-to-next-to-leading order (NNLO) in QCD for DY [75], approximately NNLO for tW [76], and NLO for WW, WZ, ZZ [77], $t\bar{t}$W and $t\bar{t}$Z [78]. For the normalization of the simulated $t\bar{t}$ sample, the full NNLO plus next-to-next-to-leading logarithmic (NNLL) accurate calculation [79], performed with the TOP++ 2.0 program [80], is used. The PDF uncertainties are added in quadrature to the uncertainty associated with the strong coupling constant (α_S) to obtain a $t\bar{t}$ production cross section of 832^{+20}_{-29} (scale) ± 35 (PDF+α_S) pb assuming $m_t = 172.5$ GeV.

The SUSY signal events are normalized to cross sections calculated at approximate NNLO+NNLL accuracy [81–90] obtained from the simplified model for the direct pair production of top squarks. The cross sections of the $t\bar{t}$ + DM model are calculated at LO using MADGRAPH v2.4.2.

4 Event reconstruction

In this section, the event reconstruction common to all the analyses presented in this paper is described.

An event may contain multiple primary vertices, corresponding to multiple pp collisions occurring in the same bunch crossing. The candidate vertex with the largest value of summed physics-object p_T^2 is taken to be the primary pp interaction vertex. The physics objects for this determination are the jets, clustered using the jet finding algorithm [91, 92] using tracks assigned to candidate vertices as inputs, and the associated missing transverse momentum, taken as the negative vector sum of the transverse momentum of those jets.

The particle-flow algorithm [93] aims to reconstruct and identify each individual particle in an event, with an optimized combination of information from the various elements of the CMS detector. The energy of photons is obtained from the ECAL measurement. The energy of electrons is determined from a combination of the electron momentum at the primary interaction vertex as determined by the tracker, the energy of the corresponding ECAL cluster, and the energy sum of all bremsstrahlung photons spatially compatible with originating from the electron track. The energy of muons is obtained from the curvature of the corresponding track. The energy of charged hadrons is determined from a combination of their momentum measured in the tracker and the matching ECAL and HCAL energy deposits, corrected for the response function of the calorimeters to hadronic showers. Finally, the energy of neutral hadrons is obtained from the corresponding corrected ECAL and HCAL energies.

For each event, hadronic jets are clustered from these reconstructed particles using the infrared and collinear safe anti-k_T algorithm [91, 92] with a distance parameter of 0.4. The jet momentum is determined as the vectorial sum of all particle momenta in the jet, and is found from simulation to be, on average, within 5 to 10% of the generated momentum over the whole p_T spectrum and detector acceptance.

Additional pp interactions within the same or nearby bunch crossings can contribute with additional tracks and calorimetric energy depositions to the jet momentum. To mitigate this effect, charged particles identified as originating from pileup vertices are discarded, and an offset correction is applied to correct for the contribution from neutral particles [94]. Jet energy corrections are derived from simulation to bring the energy of a jet measured from the detector response to that of a particle-level jet on average. In situ measurements of the momentum balance in dijet, photon+jets, Z+jets, and multijet events are used to account for any residual differences in jet energy scale between data and simulation [95]. The jet energy resolution amounts typically to 15% at 10 GeV, 8% at 100 GeV, and 4% at 1 TeV [95]. Additional selection criteria are applied to each jet to remove jets potentially dominated by anomalous contributions from various subdetector components or reconstruction failures [96]. Jets produced by the hadronization of b quarks are identified using b tagging multivariate algorithms: DeepCSV [97] for the inclusive searches and DeepJet [98, 99] for the corridor search. The more recently developed DeepJet algorithm has slightly better performance for some parts of the phase space than the DeepCSV algorithm. All analyses use a medium working point for the tagger, corresponding to a a misidentification probability for jets originating from gluons or up, down, and strange quarks of 1%, and a b tagging efficiency of about 70%. A tight working point, corresponding to a misidentification rate of 0.1%, is also used in the analysis of Section 5.2.

The missing transverse momentum vector is defined as the negative vector p_T sum of all particle-flow candidates reconstructed in an event with jet energy corrections applied. Events with serious p_T^{miss} reconstruction failures are rejected using dedicated filters [100].

The requirements imposed to select reconstructed particle objects specific to the separate search strategies incorporated into the present combination are given in the following sections. In Section 5 we give brief summaries of the previously published searches, and in Section 6 the detailed presentation of the new top quark corridor search.

5 Inclusive top squark searches

Three analyses targeting final states without leptons [16], with one [17], or with two charged leptons [18] have been previously published. The main features are briefly discussed in this section.

5.1 Fully hadronic analysis

The search in the fully hadronic final state [16] targets events with hadronic jets and large reconstructed p_T^{miss}. The SM backgrounds with intrinsic p_T^{miss} generated through the leptonic decay of a W boson, where the neutrino escapes detection, are significantly suppressed by rejecting events containing isolated electrons or muons. The contribution from events in which a W boson decays to a τ lepton is suppressed by rejecting events containing isolated hadronically decaying τ candidates [101, 102]. A central feature of this analysis is the deployment of advanced jet tagging algorithms to identify hadronically decaying top quarks and W bosons, with different algorithms covering both the highly Lorentz-boosted regime and the resolved regime. For the highly Lorentz-boosted regime, where the decay products of the particle in quest are expected to merge into a single large-R jet with a distance parameter of $R = 0.8$, the DEEPAK8 algorithm [103] is used to identify these large-R jets originating from top quarks or W bosons. In the resolved regime, where the decay products of the top quark are separately reconstructed using jets with $R = 0.4$, the DEEPRESOLVED algorithm [17] is used to tag these top quarks with intermediate p_T, ranging from 150 to 450 GeV.

To enhance sensitivity to signal models with a compressed mass spectrum where the mass of the top squark is close to the sum of the masses of the LSP and the W boson, a dedicated "soft b tag" algorithm developed to identify very low p_T b hadrons is also used for the event categorization [104]. The analysis includes a total of 183 nonoverlapping signal regions, defined in Ref. [16] and optimized for different SUSY models and ranges of mass splittings between SUSY particles. A large p_T^{miss}, due to the presence of a pair of neutralinos in the signal model, is required.

The dominant sources of SM background with intrinsic p_T^{miss} are the inclusive production of top quark pairs, W and Z bosons, single top quark production, and the $t\bar{t}Z$ process. The contribution from $t\bar{t}$, W+jets, $t\bar{t}W$, and single top quark processes arises from events in which a W boson decays leptonically to produce p_T^{miss} associated with an energetic neutrino, but the charged lepton either falls outside of the kinematic acceptance or fails the lepton identification criteria. This background is collectively referred to as "lost-lepton" background. The contributions from Z+jets and $t\bar{t}Z$ events arise when the Z boson decays to neutrinos, resulting in large genuine p_T^{miss}. Contributions from the QCD multijet process enter the search sample in cases where severe mismeasurements of jet momenta (i.e., jets passing through poorly instrumented regions of the detector) produce significant artificial p_T^{miss}, or when neutrinos arise from leptonic decays of heavy-flavor hadrons produced during the jet fragmentation. The contribution of each SM background process to the search sample is estimated through measurements of event rates in dedicated background control samples that are translated to predicted event counts in the corresponding search sample with the aid of simulation. The data are found to be in good agreement with the predicted backgrounds.

5.2 Single-lepton analysis

The search for top squark pair production in the single-lepton final state [17] focuses on final states with exactly 1 lepton, coming from the decay of a W boson from the decay chain $\widetilde{t}_1 \rightarrow t\widetilde{\chi}_1^0 \rightarrow bW\widetilde{\chi}_1^0$ or $\widetilde{t}_1 \rightarrow b\widetilde{\chi}_1^\pm \rightarrow bW\widetilde{\chi}_1^0$. Since the $\widetilde{\chi}_1^0$ in the final state of the signal gives rise to substantial p_T^{miss} compared with SM processes, $p_T^{miss} > 250\,\text{GeV}$ is required. The transverse mass computed from the lepton $\vec{p}_T$ and $\vec{p}_T^{miss}$ is required to be larger than $150\,\text{GeV}$ to reduce the lepton+jets background from $t\bar{t}$ and W+jets processes, for which m_T has a natural cutoff at the W boson mass (m_W).

The dileptonic $t\bar{t}$ process, where one of the leptons is lost, is the largest remaining SM background. In these lost-lepton events m_T is not bound by m_W because of the additional p_T^{miss} arising from the presence of a second neutrino. The modified topness (t_{mod}) variable, introduced in Ref. [17], is a measure for the likelihood of a single lepton event to originate from dileptonic $t\bar{t}$ and is used to introduce better discrimination against this background.

The dileptonic $t\bar{t}$ background is estimated through a set of dedicated control regions that require two isolated leptons. The second lepton is added to p_T^{miss} in the calculation of variables that depend on p_T^{miss}, e.g. m_T and t_{mod}, to mimic the lost-lepton scenario.

The subleading SM background comes from the process of W+jets production, where the W boson decays leptonically. While the single-lepton events from the W boson are largely suppressed by the m_T requirement, events where the W boson is produced off-shell can still enter the signal regions. The requirement of at least one b-tagged jet significantly reduces this type of background. Events are further categorized in terms of the invariant mass of the lepton and the b-tagged jet, which helps to further reduce the W+jets background. The W+jets background is estimated using control regions with an inverted b-tagged jet requirement which yields a high-purity sample of W+jets events.

Irreducible SM backgrounds arise from the $t\bar{t}Z$ and WZ processes when the Z boson decays into a pair of neutrinos. These rare backgrounds and the remaining events from the single lepton $t\bar{t}$ process are sub-dominant contributions in most search regions and are estimated using simulated samples.

This analysis also makes use of the same jet tagging algorithms, described above in the fully hadronic channel, to identify hadronic top quark decays in the final state. This is motivated by the fact that none of the leading SM backgrounds, except $t\bar{t}Z$, has a hadronically decaying top quark in the final state, while in some signal scenarios one hadronically decaying top quark is expected. Events in the lower p_T^{miss} search regions are categorized into different regions according to the presence of at least one merged or resolved top quark candidate.

Finally, a dedicated search strategy is used for signal scenarios with small mass splitting between the top squark and the LSP to optimize sensitivity. In these compressed scenarios with $\Delta m\left(\widetilde{t}_1, \widetilde{\chi}_1^0\right)$ close to m_W or m_t, p_T^{miss} can be small when neutralinos are back-to-back, and therefore t_{mod} and the merged and resolved top quark tags are not used. Instead, one non-b-tagged jet, which could arise from ISR for a signal event, is required and a requirement on the proximity of the lepton to the p_T^{miss} is introduced. In the case of $\Delta m\left(\widetilde{t}_1, \widetilde{\chi}_1^0\right) \sim m_W$ at least one "soft b tag", such as a secondary vertex, is required instead of the standard b-tagged jets, to improve the acceptance for b quarks that do not carry sufficient momentum to be reconstructed as a jet. In order to enhance the sensitivity to different signal scenarios events are categorized into 39 non-overlapping signal regions based on the values of p_T^{miss} and several of the variables introduced above.

5.3 Dilepton analysis

The search in the dilepton final state [18] is carried out using events containing a pair of leptons (electron or muons) with opposite charges. The invariant mass of the lepton pair ($m_{\ell\ell}$) is required to be greater than 20 GeV to suppress backgrounds with misidentified or nonprompt leptons from the hadronization of heavy-flavor jets in multijet events. Events with additional leptons, including candidates with looser requirements on transverse momentum, and isolation are rejected. Events with a same-flavor lepton pair that is consistent with the SM DY production are removed by requiring $|m_Z - m_{\ell\ell}| > 15$ GeV, where m_Z is the mass of the Z boson. To further suppress DY and other vector boson backgrounds, the number of jets is required to be at least two and, among them, the number of b-tagged jets to be at least one.

The p_T^{miss} significance, denoted as $\mathcal{S}$, is used to suppress events where detector effects and misreconstruction of particles from pileup interactions are the main source of reconstructed p_T^{miss}. The algorithm used to obtain $\mathcal{S}$ is described in Ref. [100]. A requirement of $\mathcal{S} > 12$ is used in order to suppress the otherwise overwhelming DY background in the same-flavor channel. This requirement exploits the stability of $\mathcal{S}$ with respect to the pileup rate for events with no genuine p_T^{miss}. The DY background is further reduced through a requirement on the azimuthal angular separation between $\vec{p}_T^{\text{miss}}$ and the momentum of the leading (subleading) jet of $\cos \Delta\phi(p_T^{\text{miss}}, \text{j}) < 0.80\,(0.96)$. These criteria reject a small background of DY events with significantly mismeasured jets.

The main variable in this analysis is $m_{\text{T2}}(\ell\ell)$, which is defined in equation (1), and extensively discussed in Ref. [23]. The key feature of the $m_{\text{T2}}(\ell\ell)$ observable is that it retains a kinematic endpoint at the W boson mass for background events from the leptonic decays of two W bosons, produced directly or through a top quark decay. Similarly, the $m_{\text{T2}}(\text{b}\ell\text{b}\ell)$ observable, defined with equation (1), but using the vector sum of the leptons and the b-jets instead of leptons alone [18], is bounded by the top quark mass if the leptons, neutrinos and b-tagged jets originate from the decay of top quarks. By contrast, signal events do not have the respective endpoints and are expected to populate the tails of these distributions.

Signal regions based on $m_{\text{T2}}(\ell\ell)$, $m_{\text{T2}}(\text{b}\ell\text{b}\ell)$, and $\mathcal{S}$ are defined to enhance the sensitivity to different signal scenarios. The regions are further divided into different categories separately for events with a same-flavor and a different-flavor lepton pair, to account for the different SM background composition. The signal regions are defined such that there is no overlap between them, nor with the background-enriched control regions.

Events with an opposite-charge lepton pair are abundantly produced by the DY and $t\bar{t}$ processes. The event selection rejects the vast majority of DY events. Therefore, the major backgrounds from SM processes in the search regions are top quark pair and single top events that pass the $m_{\text{T2}}(\ell\ell)$ threshold because of severely mismeasured p_T^{miss} or a misidentified lepton. In high $m_{\text{T2}}(\ell\ell)$ and $\mathcal{S}$ signal regions, $t\bar{t}Z$ events with $Z \to \nu\bar{\nu}$ are the main SM background. Remaining DY events with large p_T^{miss} from mismeasurement, multiboson production and other $t\bar{t}$/single t processes in association with a W, a Z or a Higgs boson ($t\bar{t}W$, tqZ, or $t\bar{t}H$) are sources of smaller contributions. A detailed description of the background estimation method is given in Ref. [18].

6 Top quark corridor analysis

The top quark corridor analysis is discussed in this section in more detail, as it is presented for the first time in this paper. In this search, events containing a dilepton pair with opposite charge

and p_T^{miss} are selected, and a DNN algorithm is used to increase the sensitivity to the signal. The full DNN score distribution for events in the signal region is used to test the presence of the signal.

6.1   Object and event selection

The object selection and baseline requirements of the event selection are the same as those for the dilepton analysis summarized in the first paragraph of Section 5.3, and are detailed in this section. Electron and muon candidates are required to have $p_T > 20\,\text{GeV}$ and $|\eta| < 2.4$. In addition, the p_T of the leading lepton must be at least $25\,\text{GeV}$. The leptons are required to be isolated by measuring their relative isolation as the scalar p_T sum, normalized to the lepton p_T, of the photons and of the neutral and charged hadrons within a cone of radius $\Delta R = \sqrt{(\Delta \eta)^2 + (\Delta \phi)^2} = 0.3\,(0.4)$ around the candidate electron (muon). In order to reduce the dependence on the number of pileup interactions, charged hadron candidates are included in the sum only if they are consistent with originating from the selected primary vertex in the event. The expected contribution from neutral hadrons due to pileup is estimated following the method described in Ref. [105]. For an electron candidate the relative isolation requirement depends on η (values close to 0.04) and for a muon it is required to be smaller than 0.15.

Selected jets are required to have $p_T > 30\,\text{GeV}$ and $|\eta| < 2.4$. Additionally, jets that are found within a cone of $\Delta R = 0.4$ around the selected leptons are rejected. Jets originating from the hadronization of bottom quarks are identified as b-tagged jets by using the medium working point of the DeepJet algorithm [98, 99].

Simulated events are corrected to account for differences with respect to data in the lepton reconstruction, identification, and isolation efficiencies, as well as efficiencies in the performance of b tagging. The values of the data-to-simulation correction factors are parameterized as functions of the p_T and η of the object and deviate from unity by less than 1% for leptons and less than 10% for b-tagged jets.

Selected events are classified in categories according to the flavor of the two leading leptons (ee, eμ, $\mu\mu$) and the data-taking period (2016, 2017, 2018). Moreover, events are required to contain at least two jets, one of which must be b tagged. This set of requirements is referred to as the baseline selection.

After the baseline selection, most of the background events (about 98%) are expected to come from $t\bar{t}$, tW, and DY processes. To suppress these backgrounds, the signal region is defined with the requirements $p_T^{miss} > 50\,\text{GeV}$ and $m_{T2}(\ell\ell) > 80\,\text{GeV}$. As described in Sec. 5.3, $m_{T2}(\ell\ell)$ serves to account for the multiple sources of p_T^{miss} in the signal process and to exploit the differences with respect to the background processes. For $t\bar{t}$, tW or W+jets events this variable's distribution has a kinematic endpoint at the W boson mass, because the transverse mass of each lepton-neutrino pair corresponds to the transverse mass of the W boson, whereas signal events have neutralinos contributing to the total p_T^{miss}, so they populate larger $m_{T2}(\ell\ell)$.

6.2   Background estimation

Although most of the $t\bar{t}$ events are rejected by requiring $m_{T2}(\ell\ell) > 80\,\text{GeV}$, it is still the dominant background contribution in the signal region, where most of the events have a large $m_{T2}(\ell\ell)$ value because of resolution effects when computing $\vec{p}_T^{\,miss}$. In this region, some of the $t\bar{t}$ events contain jets with a mismeasured energy and, in a smaller proportion, there are events where one of the leptons is missed and a lepton that is not from a W boson decay (nonprompt lepton) is taken as the second lepton in the event. The effect of the jet mismeasurements is

checked in MC and an uncertainty is assigned. Events containing nonprompt leptons are considered in a different background category.

The second-largest contribution is tW background, which is approximately 4% of the total background, and is also estimated from MC simulation. The DY events give the third-largest background contribution in the same-flavor channel, while their contribution is negligible in the eμ channel.

Background with nonprompt leptons is estimated from MC simulation and validated in a control region with the same selection as the signal region, but requiring two same-charge leptons. These events include the contribution from jets misidentified as leptons or with leptons coming from the decay of a bottom quark mistakenly identified as coming from the hard process. In the same-charge region, most of the events come from t$\bar{\text{t}}$ with nonprompt leptons, with a smaller contribution of events with prompt leptons from t$\bar{\text{t}}$W and t$\bar{\text{t}}$Z production, and dileptonic t$\bar{\text{t}}$ with prompt leptons and a mismeasurement of the electron charge. A reasonable agreement with same-charge data, within 10–15%, is observed in this validation region. Minor background contributions are also estimated from MC simulation and come from diboson (WW, WZ, and ZZ), t$\bar{\text{t}}$W, and t$\bar{\text{t}}$Z events, with a total contribution of about 1%.

The distributions of the main observables in data, the leading lepton p_{T}, $m_{\text{T2}}(\ell\ell)$, the scalar sum of the p_{T} of all the selected jets (H_{T}) and $p_{\text{T}}^{\text{miss}}$ in the signal region, are shown in Fig. 3. The simulation and data are generally in agreement within the uncertainties. The uncertainties are described in Section 6.4.

6.3 Search strategy

In order to maximize the sensitivity and to exploit all the differences between the signal and t$\bar{\text{t}}$ background, a multivariate analysis is implemented using a DNN, trained with events passing the baseline selection. The DNN takes into account all the shape differences between signal and background distributions for the training variables, including correlations, in turn achieving a strong final discriminator. The signal model used was the direct pair production of top squarks, for a sequence of $m_{\tilde{\text{t}}_1}$ mass values in the range 145–295 GeV and Δm_{cor} ranging from 0 to 30 GeV. The background input to the training was simulated t$\bar{\text{t}}$ with eμ decays. To avoid overfitting, 40% of the total t$\bar{\text{t}}$ and signal events are used for the training and the rest for the signal extraction.

The training was done using events passing the baseline selection in order to use the separation power of different observables over a large range. A total of 13 variables are selected for the training: top squark and neutralino masses ($m_{\tilde{\text{t}}_1}$, $m_{\tilde{\chi}_1^0}$), the transverse momentum of the electron-muon pair ($p_{\text{T}}^{\text{e}\mu}$), the angle between the momentum of the leptons in the transverse plane ($\Delta\phi(\text{e}\mu)$), the pseudorapidity difference between the leptons ($\Delta\eta(\text{e}\mu)$), the momenta and pseudorapidities of the individual leptons, $m_{\ell\ell}$, $m_{\text{T2}}(\ell\ell)$, $p_{\text{T}}^{\text{miss}}$, and H_{T}.

Figure 4 shows the normalized distributions of the most discriminating variables for t$\bar{\text{t}}$ and signal samples for different values of $m_{\tilde{\text{t}}_1}$ and $m_{\tilde{\chi}_1^0}$, after the baseline selection. This figure also shows that, in some variables, the shape of the distributions does not have the same behavior for all the signal points. The differences in $p_{\text{T}}^{\text{miss}}$ and $m_{\text{T2}}(\ell\ell)$ between signal and background are larger for signal points with large $m_{\tilde{\chi}_1^0}$. To exploit these differences and improve the sensitivity, a parametric DNN [39] is used, in which the top squark and neutralino masses are introduced in the training. In this way, a specific model for each signal point training a single DNN is achieved. For background events, $m_{\tilde{\text{t}}_1}$ and $m_{\tilde{\chi}_1^0}$ are randomly taken, to avoid introduc-
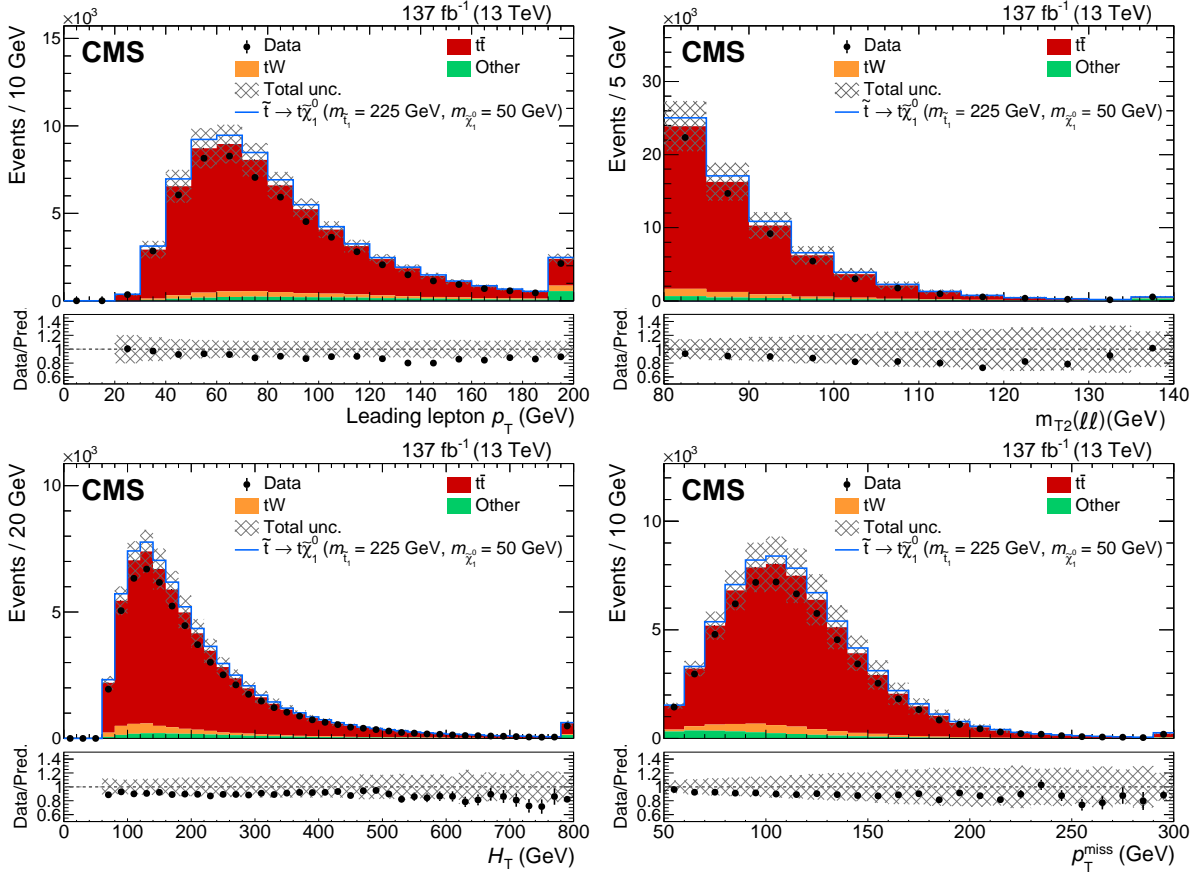
Figure 3: Pre-fit distributions of data and MC events in the signal region with the signal stacked on above the background prediction for a mass hypothesis of $m_{\tilde{t}_1} = 225\,\text{GeV}$ and $m_{\tilde{\chi}_1^0} = 50\,\text{GeV}$. Events from $t\bar{t}W$, $t\bar{t}Z$, DY, nonprompt leptons, and diboson processes are grouped into the 'Other' category. The lower panel contains the data-to-SM prediction ratio. The uncertainty band includes statistical, background normalization and all systematic uncertainties described in Section 6.4. From upper left to lower right: leading lepton p_T, $m_{T2}(\ell\ell)$, H_T, and p_T^{miss}.

ing correlations, using a probability distribution that matches the values of $m_{\tilde{t}_1}$ and $m_{\tilde{\chi}_1^0}$ in the signal sample.

The training was performed with TENSORFLOW [106] using the KERAS interface [107]. All the hyperparameters are optimized with the aim of avoiding overfitting and achieving the highest possible accuracy on the classification. The final DNN structure is sequential: 7 hidden layers with a ReLU activation function [107] (300, 200, 100, 100, 100, 100, 10 neurons). The output consists of two neurons with a softmax normalization function [107], which allows one to interpret the output numbers as probabilities. The optimizer that is selected corresponds to Adam [108] with a learning rate of 0.0001. Out of the 40% of events used for the DNN implementation, 60% are used for training, 15% for validation, and the rest to check that the DNN works properly and there is no overfitting.

Figure 5 shows the DNN output for two different mass parameters in the signal region for signal and $t\bar{t}$ background. Since both masses are introduced in the training, the DNN score shape is different for both signal and background. This figure shows that the DNN score is a good discriminator between signal and background, especially at high values of the distribution.
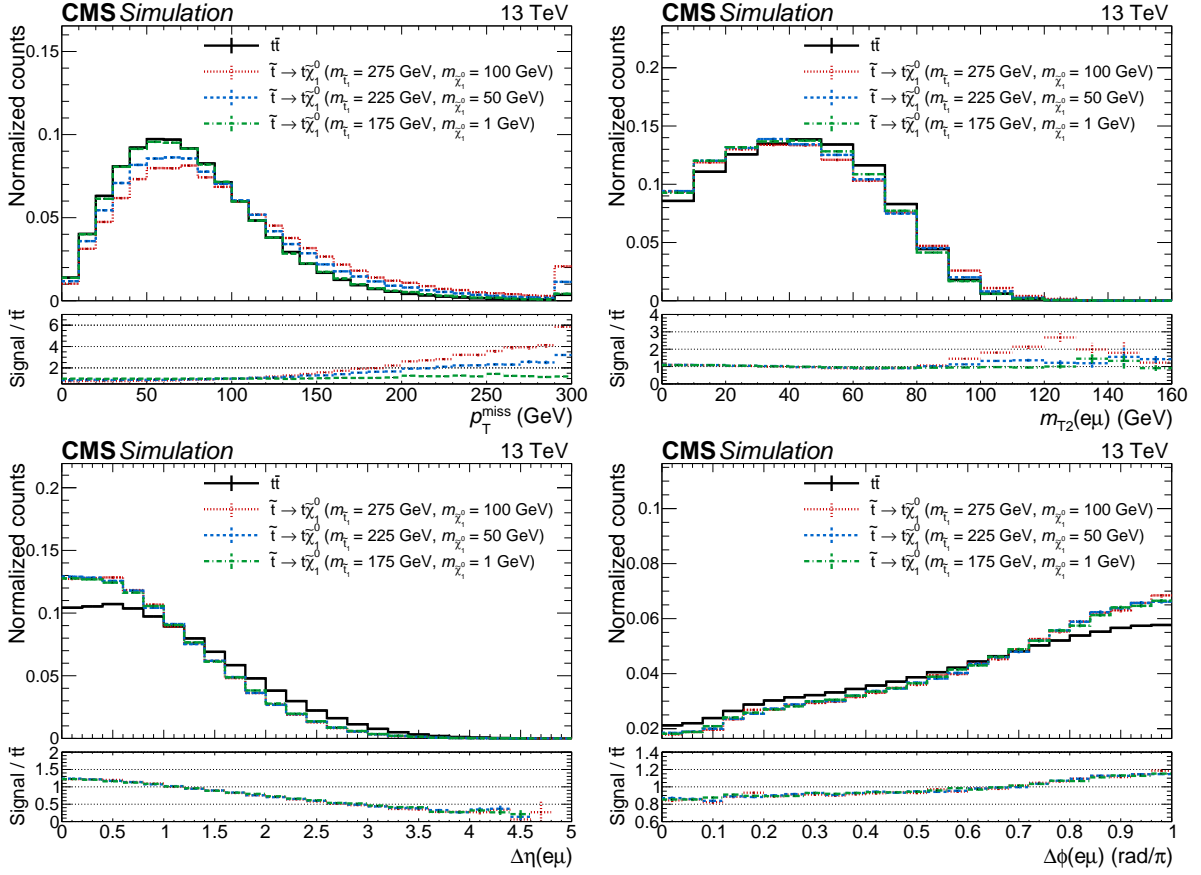
Figure 4: Normalized distributions for some of the training variables in the baseline selection. Distributions for signal points with different top squark and neutralino masses and SM $t\bar{t}$ events are compared. From upper left to lower right: p_T^{miss}, $m_{T2}(e\mu)$, $\Delta\eta(e\mu)$, and $\Delta\phi(e\mu)$.
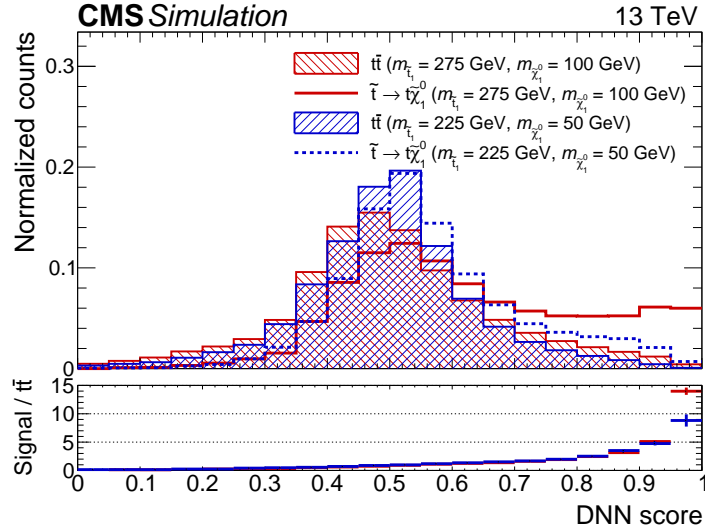

Figure 5: Normalized DNN score distribution comparing the signal and the $t\bar{t}$ background in the signal region for two mass hypotheses: $m_{\tilde{\chi}_1^0} = 50\,(100)\,\text{GeV}$ and $m_{\tilde{t}_1} = 225\,(275)\,\text{GeV}$.

The gain in sensitivity by using the DNN score instead of using only the p_T^{miss} distribution increases with increasing Δm_{cor} and with increasing $m_{\tilde{\chi}_1^0}$ for a fixed Δm_{cor}. For the fully degen-

erate case ($m_{\tilde{t}_1} = 175\,\mathrm{GeV}$, $m_{\tilde{\chi}_1^0} = 1\,\mathrm{GeV}$) the kinematics of the SUSY process are very similar to the $t\bar{t}$ background, so using the DNN does not help to improve the separation. The sensitivity to that point relies completely on the total measured cross section. For larger $m_{\tilde{t}_1}$ and $m_{\tilde{\chi}_1^0}$, even if $\Delta m_{\mathrm{cor}} = 0$, the DNN starts to improve the sensitivity (as shown in Fig. 5). The score shape separation between signal and background also starts to increase for relatively low $m_{\tilde{t}_1}$ and $m_{\tilde{\chi}_1^0}$ if $\Delta m_{\mathrm{cor}} > 0$.

The modeling of the DNN is checked in a validation region in which the signal region selection requirements are applied, except that $p_T^{\mathrm{miss}} < 50\,\mathrm{GeV}$ and $m_{\mathrm{T2}}(\ell\ell) < 80\,\mathrm{GeV}$ are required, and that only the eμ channel is used. This region is orthogonal to the signal region, and the signal contamination is expected to be small for the signal masses in which the sensitivity relies on the DNN discriminant. This region is highly dominated by $t\bar{t}$ and tW events and a good agreement with data is observed. Furthermore, the DY modeling of the DNN output distribution is also checked in a validation region where the invariant mass of the same-flavor lepton pairs is close to the mass of the Z boson. The DY background is observed to be well modeled and populates preferentially low DNN score bins.

6.4 Systematic uncertainties

Several sources of systematic uncertainty affect the background prediction and signal yields. Modeling of the trigger, efficiencies of the lepton reconstruction, identification and isolation, the jet energy scale and resolution, efficiencies of the b tagging and mistag rate, and the pileup modeling have uncertainties that are considered in the estimate of both background and signal yields. All these sources are described in Section 6.4.1.

As the $t\bar{t}$ background plays an essential role and needs to be accurately estimated, various modeling uncertainties are taken into account. These uncertainties consider variations of the main theoretical parameters used in the simulation and have been studied previously by the CMS Collaboration [62, 63]. These uncertainties are explained in detail in Section 6.4.2.

Uncertainties in signal modeling are described in Section 6.4.3. Section 6.4.4 includes other sources of uncertainty as the background and signal normalization uncertainties.

6.4.1 Experimental uncertainties

The following experimental uncertainties are calculated for every background and signal estimate and are propagated to the final DNN output distribution in the signal region.

The uncertainties in the trigger, lepton identification, and isolation efficiencies used in simulation are estimated by varying data-to-simulation scale factors by their uncertainties, which are about 1.5% for electron identification and isolation efficiencies, 1% for muon identification and isolation efficiencies, and about 1.5% for the trigger efficiency. The uncertainties in the muon momentum scales are taken into account by varying the momenta of the muons by their uncertainties, taken from the muon momentum scale corrections [109]. All these uncertainties are considered as correlated between years.

For the b tagging efficiency and mistag rate the uncertainties are determined by varying the scale factors for the b-tagged jets and mistagged light-flavor quark and gluon jets, according to their uncertainties, as measured in QCD multijet events [97–99]. The uncertainties related to the jet energy scale and jet energy resolution are calculated by varying these quantities in bins of p_T and η, according to the uncertainties in the jet energy corrections, which amount to a few percent [95]. The uncertainty in the effect of the jet mismeasurements, described in

Section 6.2, is added to the jet energy resolution uncertainties. This uncertainty is taken as partially correlated between years.

The uncertainty in p_T^{miss} from the contribution of unclustered energy is evaluated based on the momentum resolution of the different particle-flow candidates, according to their classification. Details on the procedure can be found in Refs. [93, 110, 111]. The uncertainty in the modeling of the contributions from pileup collisions is evaluated by varying the inelastic pp cross section in the simulation by $\pm 4.6\%$ [112]. These uncertainties are treated as correlated between data periods.

A summary of the experimental uncertainties in the $t\bar{t}$ background and signal is shown in Table 1. These uncertainties are also applied to the prediction of other minor backgrounds and have an effect in both the shape and the normalization.

Table 1: Summary of the contributions of the experimental uncertainties in the DNN score distribution for signal and the $t\bar{t}$ background. The values represent the relative variation in the number of expected events across different signal models in the signal region.

Source	Uncertainties (%)	
	$t\bar{t}$	signal
Electron efficiency	1.5	
Muon efficiency	0.5	
Trigger modeling	1.2	
Muon energy scale	1.4	
b tagging efficiency	3.0	
Jet energy resolution	16.0	7.0
Jet energy scale	7.5	5.7
Unclustered energy	4.2	5.0
Pileup modeling	3.2	1.5
Size of the MC sample	3.0	25.0

6.4.2 Modeling uncertainties in the $t\bar{t}$ background

Modeling uncertainties for the $t\bar{t}$ background are calculated by varying different theoretical parameters in the MC generator within their uncertainties and propagating their effect to the final distributions.

The uncertainty in the modeling of the hard-interaction process is assessed in the POWHEG sample varying up and down μ_F and μ_R by factors of 2 and 1/2 relative to their common nominal value of $\mu_F^2 = \mu_R^2 = m_t^2 + p_{T,t}^2$. Here $p_{T,t}$ denotes the p_T of the top quark in the $t\bar{t}$ rest frame. The effect of this variation is propagated to the acceptance and efficiency, estimated using the $t\bar{t}$ POWHEG sample. This uncertainty is correlated among the data-taking periods.

The uncertainty in the choice of the PDFs and in the value of α_S is determined by reweighting the sample of simulated $t\bar{t}$ events according to the envelope of a PDF set of 100 NNPDF3.0 replicas [67] for 2016 and 32 PDF4LHC replicas [113] for 2017 and 2018. The uncertainty in α_S is propagated to the acceptance by reweighting the simulated sample by sets of weights with two variations within the uncertainties of α_S. Only the uncertainties for the 2017 and 2018 periods are taken to be correlated, while the 2016 period is kept uncorrelated, because the PDF set used is different.

The effect of the modeling uncertainties of the initial-state and final-state radiation is evaluated by varying the parton shower scales (running α_S) by factors of 2 and 1/2 [59]. In addition,

the impact of the matrix element and parton shower matching, which is parameterized by the POWHEG generator as $h_{\text{damp}} = 1.58^{+0.66}_{-0.59} \, m_{\text{t}}$ [63, 64], is calculated by varying this parameter within the uncertainties. This uncertainty is calculated using dedicated $t\bar{t}$ samples and is taken as correlated between the years.

To model the measured underlying event the parameters of PYTHIA are tuned [64, 70]. An uncertainty is assigned by varying these parameters within their uncertainties using dedicated $t\bar{t}$ samples. The uncertainty corresponding to the 2016 period is applied for the CUETP8M2T4 tune and is kept as uncorrelated to the uncertainty on the CP5 tune for 2017 and 2018, which is fully correlated for the two periods.

An uncertainty on the p_{T} of the top quark is also considered to account for the known mismodeling found in the POWHEG MC sample [63]. A reweighting procedure exists to fix the mismodeling but, to avoid biasing the search, we use unweighted distributions and assign an uncertainty from the full difference to the weighted distributions.

For the top quark mass, 1 GeV is conservatively taken as the uncertainty, which corresponds to twice the uncertainty of the CMS measurement [114], and is also propagated to the acceptance. The differences in the final yields for each bin of the DNN score distribution between the $t\bar{t}$ background prediction with $m_{\text{t}} = 172.5 \pm 1.0$ GeV are taken as an uncertainty, accounting for the possible bias introduced in the choice of $m_{\text{t}} = 172.5$ GeV in the MC simulation. The uncertainty is assessed using dedicated $t\bar{t}$ samples produced with a different m_{t}.

The modeling uncertainties in the signal region yields for the $t\bar{t}$ background are summarized in Table 2; they have an effect on the shape and also on the normalization.

Table 2: Summary of the contribution of each modeling uncertainty source to the DNN score distribution for the $t\bar{t}$ background.

Source	Average for $t\bar{t}$ (%)
PDFs and α_{S} (acceptance)	1.0
μ_{F}, μ_{R} scales (acceptance)	3.8
Initial-state radiation	0.6
Final-state radiation	3.4
Top p_{T}	1.3
Matrix element/parton shower matching	2.0
Underlying event	1.5
Top quark mass (acceptance)	1.5

6.4.3   Signal modeling

The effect on the signal model of the ISR reweighting, described in Section 3, is considered. Half of the deviation from unity is taken as the systematic uncertainty in these reweighting factors. This uncertainty is propagated to the final distribution and taken as a shape uncertainty.

The uncertainty in the modeling of the hard interaction in the simulated signal sample is calculated varying up and down μ_{F} and μ_{R} by factors of 2 and 1/2 relative to their nominal value. In addition, a 6.5% uncertainty in the signal normalization is assigned, according to the uncertainties in the predicted cross section of signal models in the top squark mass range of the analysis [87].

6.4.4 Other uncertainties

The uncertainty in the overall integrated luminosity for the combined sample, which affects the signal and background normalization, amounts to 1.6% [115–118]. The total uncertainty is split in different sources, partially correlated across years.

A normalization uncertainty is applied to each background and signal estimate separately. The uncertainty in the $t\bar{t}$ normalization is taken from the uncertainty in the NNLO+NNLL cross section, as quoted in Section 3, and additionally the top quark mass is varied by ± 1 GeV, leading to a variation of the cross section of 6%.

For DY, dibosons, $t\bar{t}W$, and $t\bar{t}Z$ processes a 30% normalization uncertainty is assigned covering the uncertainty in the theoretical cross section and in the measurements. For the tW process an uncertainty of 12% is assigned. In the case of the nonprompt lepton background, a normalization uncertainty of 30% is also applied, covering the largest deviations observed in the same-charge control region described in Section 6.2.

Statistical uncertainties arise from the limited size of the MC samples. They are considered for each signal and background process, in each bin of the distributions. They are introduced through the Barlow–Beeston approach [119].

All the systematic uncertainties described in Sections 6.4.1 and 6.4.2 are assigned to each DNN distribution bin individually, and treated as correlated among all the bins and all processes. The statistical uncertainties are treated as uncorrelated nuisance parameters in each bin of the DNN score distribution. All of the systematic uncertainties are treated as fully correlated among the different final states.

7 Results

7.1 Corridor results

The statistical interpretation is performed by testing the SM hypothesis against the SUSY hypothesis. The data and predicted distributions for the DNN response in the signal region are combined in the nine channels (3 data-taking period x 3 lepton flavor combinations of the two leading leptons) in order to maximize the sensitivity to the signal. Each of the distributions is computed for different values of the mass parameters and compared to the prediction for the signal model with the corresponding masses. In Fig. 6 the DNN score distributions for data are compared with those from the fit. The fit function includes the background, and the signal prediction scaled by the post-fit signal strength, for different mass parameters. The points whose DNN distributions appear in the upper plots lie along the center line of the corridor, $\Delta m_{\mathrm{cor}} = 0$, while those shown in the lower plots lie on its boundary.

A binned profile likelihood fit of the DNN output distribution is performed, where the nuisance parameters are modeled using Gaussian distributions. The correlation scheme for different data periods is described in Section 6.4. No significant excess is observed over the background prediction for any of the distributions.

Upper limits on the production cross section of top squark pairs are calculated at 95% confidence level (CL) using a modified frequentist approach and the $\mathrm{CL_s}$ criterion, implemented through an asymptotic approximation [120–123].

Results are interpreted for different signals characterized by $145 < m_{\tilde{t}_1} < 295$ GeV and $\Delta m_{\mathrm{cor}} \leq 30$ GeV. The observed upper limit on the signal cross section is shown in Fig. 7. The ex-
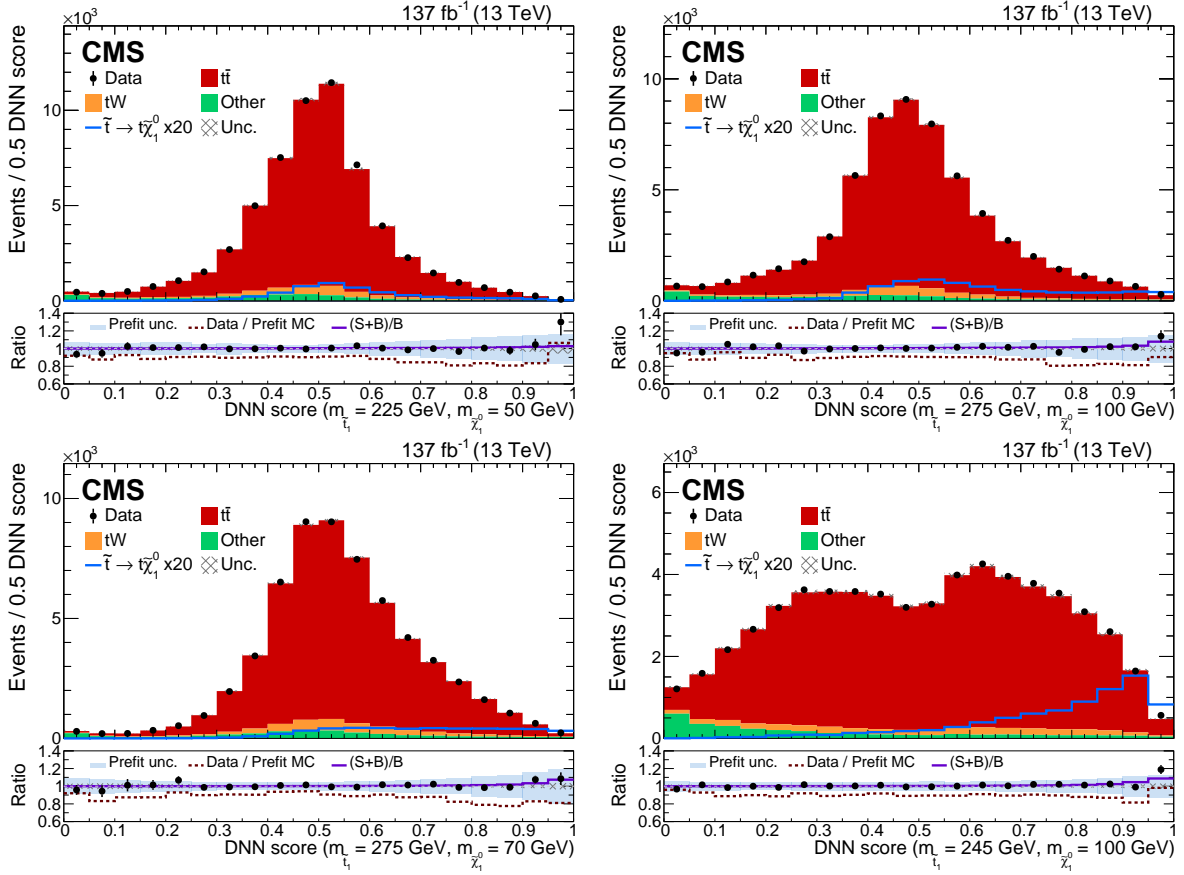
Figure 6: Post-fit DNN score distributions in the signal region for different mass hypotheses of, from upper left to lower right, $(m_{\tilde{t}_1}, m_{\tilde{\chi}_1^0}) = (225, 50); (275, 100); (275, 70);$ and $(245, 100)$ GeV. The superimposed signal prediction is scaled by the post-fit signal strength and, in the upper panels, it is also multiplied by a factor 20 for better visibility. The post-fit uncertainty band (crosses) includes statistical, background normalization, and all systematic uncertainties described in Section 6.4. Events from $t\bar{t}W$, $t\bar{t}Z$, DY, nonprompt leptons, and diboson processes are grouped into the 'Other' category. The lower panel contains the data-to-prediction ratio before the fit (dotted brown line) and after (dots), each of them with their corresponding band of uncertainties (blue band for the pre-fit and crosses band for the post-fit). The ratio between the sum of the signal and background predictions and the background prediction (purple line) is also shown. The masses of the signal model correspond to the values of the DNN mass parameters in each distribution.

pected and observed upper limits are also shown for three different slices corresponding to $\Delta m (\tilde{t}_1, \tilde{\chi}_1^0) = 165, 175$ and 185 GeV in Fig. 8. Both the observed and expected cross section limits exclude the model over the region of the search.

7.2 Combined results

A statistical combination of the results of the three searches described in detail in Section 5 is performed outside the corridor area in order to provide interpretations in the context of the signal scenarios described in Section 1. The signal regions of the analyses targeting different final states are designed to be mutually exclusive. Additionally, there is no significant overlap of any of the control regions with signal regions of a different analysis. The overlap between control regions of the single-lepton and dilepton analysis is found to be less than 1% and there-
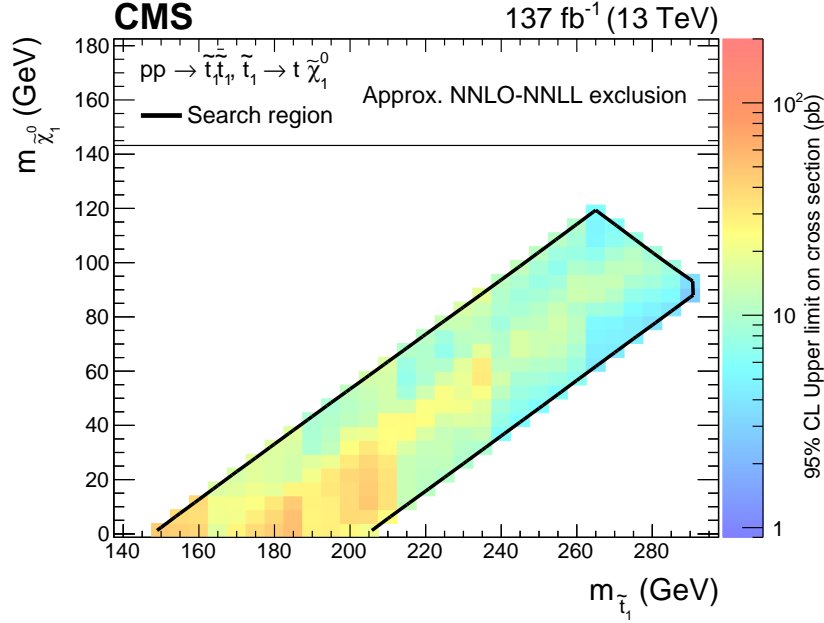
Figure 7: Upper limit at 95% CL on the signal cross section as a function of the top squark and neutralino masses in the top quark corridor region. The model is excluded for all of the colored region inside the black boundary.

fore considered negligible. Correlations of systematic uncertainties in the expected signal and background yields are studied and taken into account. Uncertainties in the jet energy scale and p_T^{miss} resolution, b tagging efficiency scale factors, heavy resonance taggers, integrated luminosity and background normalizations are treated as fully correlated. Because of differences in the lepton identification methods and working points, as well as the triggers to select events, the corresponding uncertainties are considered uncorrelated. Theory uncertainties in the choice of the PDF, μ_R and μ_F and ISR modeling of the signal prediction, as well as SM backgrounds that are estimated using simulation, are taken to be fully correlated.

Figure 9 (upper left) shows the combination of the results of the three searches for direct top squark pair production for the model with $\tilde{t}_1 \rightarrow t\tilde{\chi}_1^0$ decays. The analysis described in Section 6 is exclusively used for extracting limits in the top quark corridor region. No result of the other analyses is used in this particular region of parameter space. The combined result excludes a top squark mass of 1325 GeV for a massless LSP, and an LSP mass of 700 GeV for a top squark mass of 1150 GeV. The expected limit of the combination is dominated by the fully hadronic search for signals with large mass splitting. In regions with smaller mass splitting between the top squark and the LSP, searches in the zero- and single-lepton channels have similar sensitivity.

Figure 9 (upper right) shows the equivalent limits for direct top squark pair production for the model with $\tilde{t}_1 \rightarrow b\tilde{\chi}_1^+ \rightarrow bW^+\tilde{\chi}_1^0$ decays. The mass of the chargino is set to the mean of the masses of the top squark and the LSP. The combined result for this scenario excludes a top squark mass of 1260 GeV for a massless LSP and an LSP mass of 575 GeV for a top squark mass of 1000 GeV. The combination extends the sensitivity to both top squark and LSP masses by about 50 GeV compared to the most sensitive individual result coming from the fully hadronic channel.

Figure 9 (lower) shows the limits for the model with a 50% branching fraction of the top squark decays discussed previously. In this model, the mass splitting between the neutralino and chargino is assumed to be 5 GeV. Because of the low acceptance for low-momentum leptons
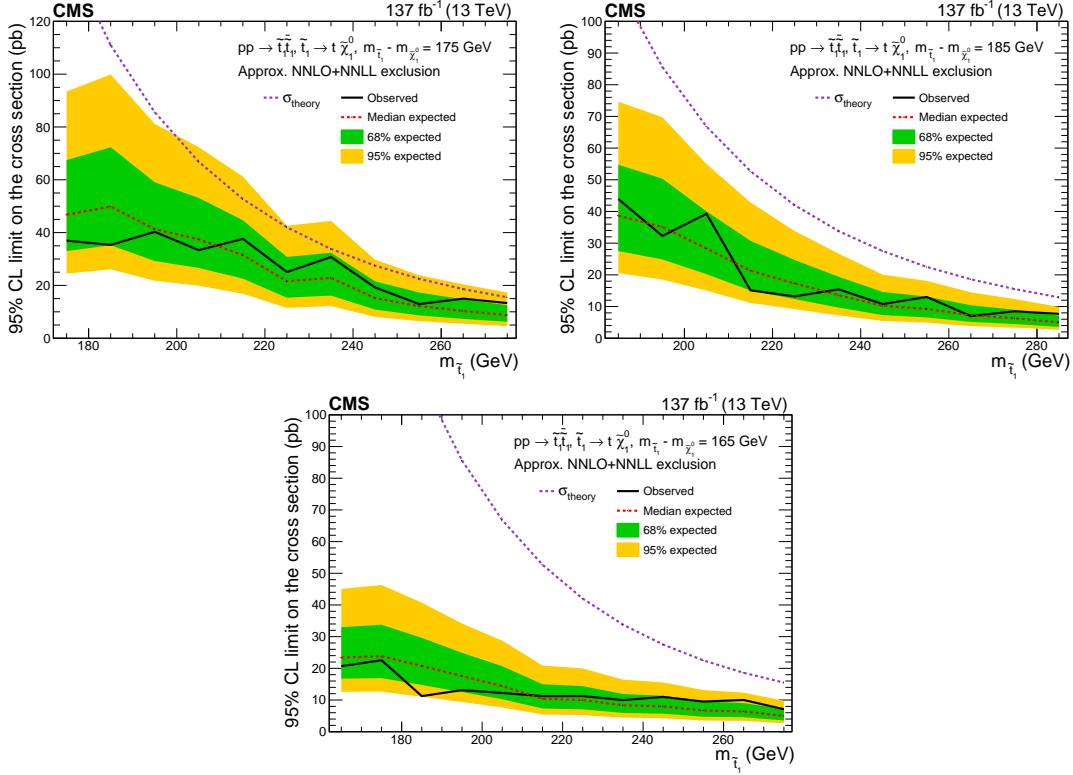
Figure 8: Upper limit at 95% CL on the signal cross section as a function of the top squark mass for $\Delta m \left(\tilde{t}_1, \tilde{\chi}_1^0 \right)$ of 175 GeV (upper left), 185 GeV (upper right) and 165 GeV (lower). The green and yellow bands represent the regions containing 68 and 95%, respectively, of the distribution of limits expected under the background-only hypothesis. The purple dotted line indicates the approximate NNLO+NNLL production cross section.

the dilepton result is not interpreted in terms of this model. Top squark masses up to 1175 GeV are excluded in this model when the LSP is massless, and up to 1000 GeV for LSP masses up to 570 GeV.

As shown in Fig. 9 (upper left), the region of the parameter space of the simplified SUSY models considered for interpretation in this analysis, which is favored by the naturalness paradigm, is now further constrained by the exclusion limits.

7.3   Search for dark matter in association with top quarks

The results of the inclusive top squark searches are interpreted in simplified models of associated production of DM particles with a top quark pair, shown in Fig. 2. The interaction of the DM particles and the top quark is mediated by a scalar or pseudoscalar mediator particle. Assuming a dark matter particle mass of 1 GeV, scalar and pseudoscalar mediators with masses up to 400 and 420 GeV are excluded at 95% CL, respectively, as shown in Fig. 10. The obtained upper limits on $\sigma(pp \rightarrow t\bar{t}\chi\tilde{\chi}) / \sigma_{\text{theory}}$ are independent of the mass of the DM fermion (m_χ), as long as the mediator is produced on-shell [46]. Previous results are improved by more than 100 GeV [50, 51] and the sensitivity extends beyond $m_{\phi/a} > 2m_t$ for the first time. The competing decay channel of the mediator into a top quark pair, $\phi/a \rightarrow t\bar{t}$, is taken into account in the signal simulation and cross section calculation.
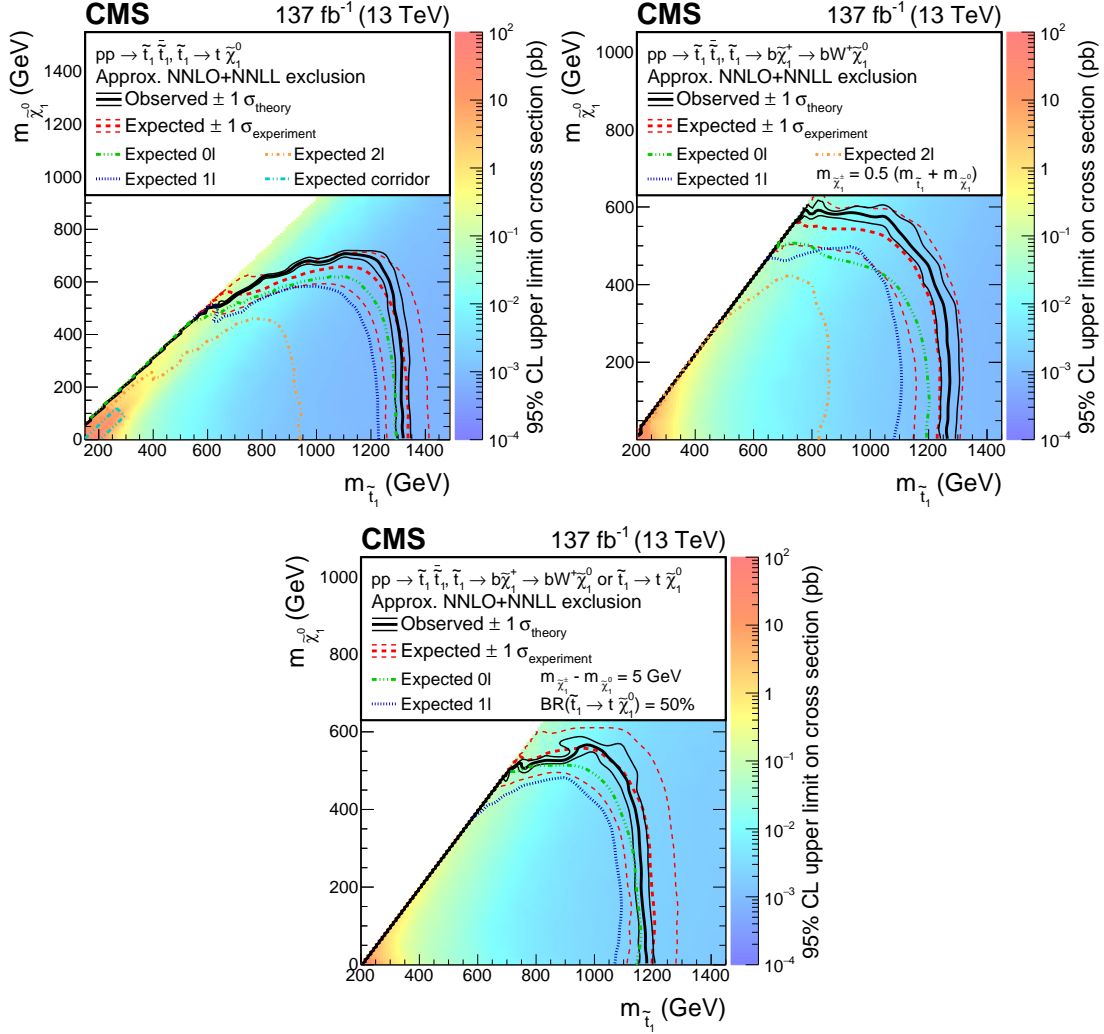
Figure 9: Expected and observed limits in the $m_{\tilde{t}_1}$-$m_{\tilde{\chi}_1^0}$ mass plane, for the $\tilde{t}_1 \to t\tilde{\chi}_1^0$ model (upper left), the $\tilde{t}_1 \to b\tilde{\chi}_1^+ \to bW^+\tilde{\chi}_1^0$ model (upper right) and a model with a branching fraction of 50% for each of these top squark decay modes (lower), assuming a mass difference between the neutralino and chargino of 5 GeV. The color indicates the 95% CL upper limit on the cross section at each point in the plane. The area below the thick black curve represents the observed exclusion region at 95% CL, while the dashed red lines indicate the expected limits at 95% CL and the region containing 68% of the distribution of limits expected under the background-only hypothesis of the combined analyses. The thin black lines show the effect of the theoretical uncertainties in the signal cross section.

8 Summary

Four searches for top squark pair production and their statistical combination are presented. The searches use a data set of proton-proton collisions at a center-of-mass energy of 13 TeV collected by the CMS detector and corresponding to an integrated luminosity of 137 fb^{-1}. A dedicated analysis is presented that is sensitive to signal models where the mass splitting between the top squark and the lightest supersymmetric particle (LSP) is close to the top quark mass. A deep neural network algorithm is used to separate the signal from the top quark background using events containing an opposite-charge dilepton pair, at least two jets, at least one b-tagged jet, $p_T^{miss} > 50$ GeV, and stransverse mass greater than 80 GeV. No excess of data over
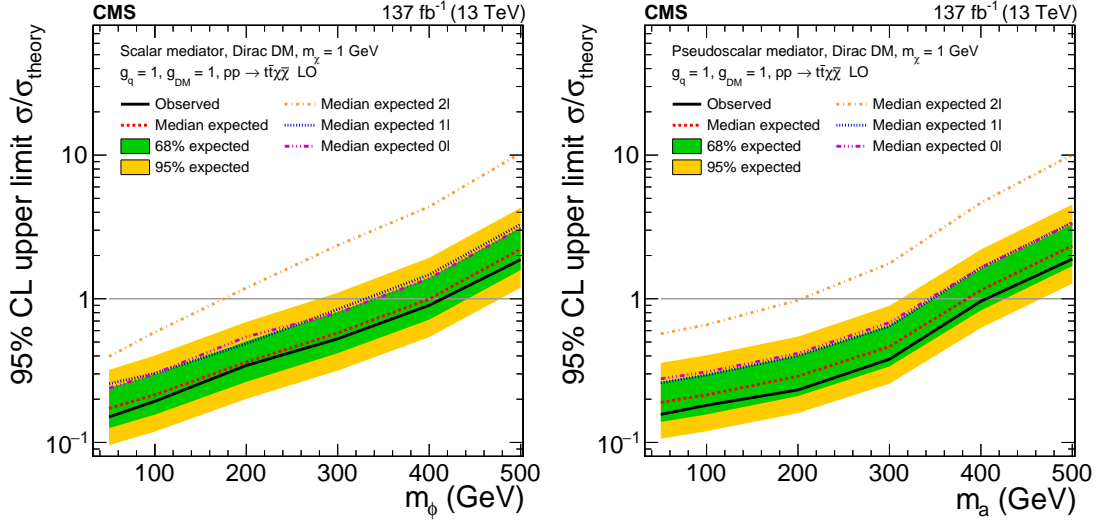
Figure 10: The 95% CL expected (dashed line) and observed limits (solid line) on $\sigma/\sigma_{\text{theory}}$ for a fermionic DM particle with $m_\chi = 1\,\text{GeV}$, as a function of the mediator mass for a scalar (left) and pseudoscalar (right). The green and yellow bands represent the regions containing 68 and 95%, respectively, of the distribution of limits expected under the background-only hypothesis. The horizontal gray line indicates $\sigma/\sigma_{\text{theory}} = 1$. The mediator couplings are set to $g_q = g_{\text{DM}} = 1$.

the standard model prediction is observed, and upper limits are set at 95% confidence level on the top squark production cross section. Top squarks with mass from 145 to 275 GeV, for LSP mass from 0 to 100 GeV, with a mass difference between the top squarks and LSP of up to 30 GeV deviation around the mass of the top quark, are excluded for the first time in CMS. Previously published searches in final states with 0, 1, or 2 leptons are combined to extend the exclusion limits of top squarks with masses up to 1325 GeV for a massless LSP and an LSP mass up to 700 GeV for a top squark mass of 1150 GeV, for certain models of top squark production. In an alternative signal model of dark matter production via a spin-0 mediator in association with a top quark pair, mediator particle masses up to 400 and 420 GeV are excluded for scalar or pseudoscalar mediators, respectively, assuming a dark matter particle mass of 1 GeV.

Acknowledgments

References

[1] R. Barbieri and G. F. Giudice, "Upper bounds on supersymmetric particle masses", *Nucl. Phys. B* **306** (1988) 63, `doi:10.1016/0550-3213(88)90171-X`.

[2] E. Witten, "Dynamical breaking of supersymmetry", *Nucl. Phys. B* **188** (1981) 513, `doi:10.1016/0550-3213(81)90006-7`.

[3] G. Bertone, D. Hooper, and J. Silk, "Particle dark matter: evidence, candidates and constraints", *Phys. Rept.* **405** (2005) 279, `doi:10.1016/j.physrep.2004.08.031`, `arXiv:1304.0790`.

[4] J. L. Feng, "Dark matter candidates from particle physics and methods of detection", *Ann. Rev. Astron. Astrophys.* **48** (2010) 495, `doi:10.1146/annurev-astro-082708-101659`, `arXiv:1003.0904`.

[5] P. Ramond, "Dual theory for free fermions", *Phys. Rev. D* **3** (1971) 2415, `doi:10.1103/PhysRevD.3.2415`.

[6] Y. A. Golfand and E. P. Likhtman, "Extension of the algebra of Poincaré group generators and violation of P invariance", *JETP Lett.* **13** (1971) 323.

[7] A. Neveu and J. H. Schwarz, "Factorizable dual model of pions", *Nucl. Phys. B* **31** (1971) 86, `doi:10.1016/0550-3213(71)90448-2`.

[8] D. V. Volkov and V. P. Akulov, "Possible universal neutrino interaction", *JETP Lett.* **16** (1972) 438.

[9] J. Wess and B. Zumino, "A Lagrangian model invariant under supergauge transformations", *Phys. Lett. B* **49** (1974) 52, `doi:10.1016/0370-2693(74)90578-4`.

[10] J. Wess and B. Zumino, "Supergauge transformations in four-dimensions", *Nucl. Phys. B* **70** (1974) 39, `doi:10.1016/0550-3213(74)90355-1`.

[11] P. Fayet, "Supergauge invariant extension of the Higgs mechanism and a model for the electron and its neutrino", *Nucl. Phys. B* **90** (1975) 104, `doi:10.1016/0550-3213(75)90636-7`.

[12] H. P. Nilles, "Supersymmetry, supergravity and particle physics", *Phys. Rept.* **110** (1984) 1, `doi:10.1016/0370-1573(84)90008-5`.

[13] A. E. Faraggi and M. Pospelov, "Selfinteracting dark matter from the hidden heterotic string sector", *Astropart. Phys.* **16** (2002) 451, `doi:10.1016/S0927-6505(01)00121-9`, `arXiv:hep-ph/0008223`.

[14] R. Barbieri and D. Pappadopulo, "S-particles at their naturalness limits", *JHEP* **10** (2009) 061, `doi:10.1088/1126-6708/2009/10/061`, `arXiv:0906.4546`.

[15] M. Papucci, J. T. Ruderman, and A. Weiler, "Natural SUSY endures", *JHEP* **09** (2012) 035, `doi:10.1007/JHEP09(2012)035`, `arXiv:1110.6926`.

[16] CMS Collaboration, "Search for top squark production in fully-hadronic final states in proton-proton collisions at $\sqrt{s} = 13$ TeV", *Phys. Rev. D* **104** (2021) 052001, `doi:10.1103/PhysRevD.104.052001`, `arXiv:2103.01290`.

[17] CMS Collaboration, "Search for direct top squark pair production in events with one lepton, jets, and missing transverse momentum at 13 TeV with the CMS experiment", *JHEP* **05** (2020) 032, `doi:10.1007/JHEP05(2020)032`, `arXiv:1912.08887`.

[18] CMS Collaboration, "Search for top squark pair production using dilepton final states in pp collision data collected at $\sqrt{s} = 13$ TeV", *Eur. Phys. J. C* **81** (2021) 3, `doi:10.1140/epjc/s10052-020-08701-5`, `arXiv:2008.05936`.

[19] J. Alwall, P. Schuster, and N. Toro, "Simplified models for a first characterization of new physics at the LHC", *Phys. Rev. D* **79** (2009) 075020, `doi:10.1103/PhysRevD.79.075020`, `arXiv:0810.3921`.

[20] J. Alwall, M.-P. Le, M. Lisanti, and J. G. Wacker, "Model-independent jets plus missing energy searches", *Phys. Rev. D* **79** (2009) 015005, `doi:10.1103/PhysRevD.79.015005`, `arXiv:0809.3264`.

[21] LHC New Physics Working Group, "Simplified models for LHC new physics searches", *J. Phys. G* **39** (2012) 105005, `doi:10.1088/0954-3899/39/10/105005`, `arXiv:1105.2838`.

[22] CMS Collaboration, "Search for top squark pair production in pp collisions at $\sqrt{s} = 13$ TeV using single lepton events", *JHEP* **10** (2017) 019, `doi:10.1007/JHEP10(2017)019`, `arXiv:1706.04402`.

[23] CMS Collaboration, "Search for top squarks and dark matter particles in opposite-charge dilepton final states at $\sqrt{s} = 13$ TeV", *Phys. Rev. D* **97** (2018) 032009, `doi:10.1103/PhysRevD.97.032009`, `arXiv:1711.00752`.

[24] CMS Collaboration, "Search for top-squark pair production in the single-lepton final state in pp collisions at $\sqrt{s} = 8$ TeV", *Eur. Phys. J. C* **73** (2013) 2677, `doi:10.1140/epjc/s10052-013-2677-2`, `arXiv:1308.1586`.

[25] CMS Collaboration, "Search for direct pair production of scalar top quarks in the single- and dilepton channels in proton-proton collisions at $\sqrt{s} = 8$ TeV", *JHEP* **07** (2016) 027, `doi:10.1007/JHEP07(2016)027`, `arXiv:1602.03169`. [Erratum: `doi:10.1007/JHEP09(2016)056`].

[26] CMS Collaboration, "Search for top squark pair production in compressed-mass-spectrum scenarios in proton-proton collisions at $\sqrt{s} = 8$ TeV using the α_T variable", *Phys. Lett. B* **767** (2017) 403, `doi:10.1016/j.physletb.2017.02.007`, `arXiv:1605.08993`.

[27] CMS Collaboration, "Searches for pair production of third-generation squarks in $\sqrt{s} = 13$ TeV pp collisions", *Eur. Phys. J. C* **77** (2017) 327, `doi:10.1140/epjc/s10052-017-4853-2`, `arXiv:1612.03877`.

[28] CMS Collaboration, "Search for direct production of supersymmetric partners of the top quark in the all-jets final state in proton-proton collisions at $\sqrt{s} = 13$ TeV", *JHEP* **10** (2017) 005, `doi:10.1007/JHEP10(2017)005`, `arXiv:1707.03316`.

[29] CMS Collaboration, "Search for supersymmetry in proton-proton collisions at 13 TeV using identified top quarks", *Phys. Rev. D* **97** (2018) 012007, `doi:10.1103/PhysRevD.97.012007`, `arXiv:1710.11188`.

[30] ATLAS Collaboration, "Search for new phenomena in events with two opposite-charge leptons, jets and missing transverse momentum in pp collisions at $\sqrt{s} = 13$ TeV with the ATLAS detector", *JHEP* **04** (2021) 165, `doi:10.1007/JHEP04(2021)165`, `arXiv:2102.01444`.

[31] ATLAS Collaboration, "ATLAS Run 1 searches for direct pair production of third-generation squarks at the Large Hadron Collider", *Eur. Phys. J. C* **75** (2015) 510, `doi:10.1140/epjc/s10052-015-3726-9`, `arXiv:1506.08616`. [Erratum: `doi:10.1140/epjc/s10052-016-3935-x`].

[32] ATLAS Collaboration, "Search for top squark pair production in final states with one isolated lepton, jets, and missing transverse momentum in $\sqrt{s} = 8$ TeV pp collisions with the ATLAS detector", *JHEP* **11** (2014) 118, `doi:10.1007/JHEP11(2014)118`, `arXiv:1407.0583`.

[33] ATLAS Collaboration, "Search for direct top-squark pair production in final states with two leptons in pp collisions at $\sqrt{s} = 8$ TeV with the ATLAS detector", *JHEP* **06** (2014) 124, `doi:10.1007/JHEP06(2014)124`, `arXiv:1403.4853`.

[34] ATLAS Collaboration, "Search for new phenomena with top quark pairs in final states with one lepton, jets, and missing transverse momentum in pp collisions at $\sqrt{s} = 13$ TeV with the ATLAS detector", *JHEP* **04** (2021) 174, `doi:10.1007/JHEP04(2021)174`, `arXiv:2012.03799`.

[35] ATLAS Collaboration, "Search for a scalar partner of the top quark in the all-hadronic $t\bar{t}$ plus missing transverse momentum final state at $\sqrt{s} = 13$ TeV with the ATLAS detector", *Eur. Phys. J. C* **80** (2020) 737, `doi:10.1140/epjc/s10052-020-8102-8`, `arXiv:2004.14060`.

[36] CMS Collaboration, "Measurement of the $t\bar{t}$ production cross section in the eμ channel in proton-proton collisions at $\sqrt{s} = 7$ and 8 TeV", *JHEP* **08** (2016) 029, `doi:10.1007/JHEP08(2016)029`, `arXiv:1603.02303`.

[37] CMS Collaboration, "Search for the pair production of light top squarks in the e$^{\pm}\mu^{\mp}$ final state in proton-proton collisions at $\sqrt{s} = 13$ TeV", *JHEP* **03** (2019) 101, `doi:10.1007/JHEP03(2019)101`, `arXiv:1901.01288`.

[38] ATLAS Collaboration, "Measurements of top-quark pair spin correlations in the $e\mu$ channel at $\sqrt{s} = 13$ TeV using pp collisions in the ATLAS detector", *Eur. Phys. J. C* **80** (2020) 754, `doi:10.1140/epjc/s10052-020-8181-6`, `arXiv:1903.07570`.

[39] P. Baldi et al., "Parameterized neural networks for high-energy physics", *Eur. Phys. J. C* **76** (2016) 235, `doi:10.1140/epjc/s10052-016-4099-4`, `arXiv:1601.07913`.

[40] C. G. Lester and D. J. Summers, "Measuring masses of semi-invisibly decaying particles pair produced at hadron colliders", *Phys. Lett. B* **463** (1999) 99, `doi:10.1016/S0370-2693(99)00945-4`, `arXiv:hep-ph/9906349`.

[41] H.-C. Cheng and Z. Han, "Minimal kinematic constraints and m_{T2}", *JHEP* **12** (2008) 063, `doi:10.1088/1126-6708/2008/12/063`, `arXiv:0810.5178`.

[42] T. Lin, E. W. Kolb, and L.-T. Wang, "Probing dark matter couplings to top and bottom quarks at the LHC", *Phys. Rev. D* **88** (2013) 063510, `doi:10.1103/PhysRevD.88.063510`, `arXiv:1303.6638`.

[43] M. R. Buckley, D. Feld, and D. Goncalves, "Scalar simplified models for dark matter", *Phys. Rev. D* **91** (2015) 015017, `doi:10.1103/PhysRevD.91.015017`, `arXiv:1410.6497`.

[44] U. Haisch and E. Re, "Simplified dark matter top-quark interactions at the LHC", *JHEP* **06** (2015) 078, `doi:10.1007/JHEP06(2015)078`, `arXiv:1503.00691`.

[45] C. Arina et al., "A comprehensive approach to dark matter studies: exploration of simplified top-philic models", *JHEP* **11** (2016) 111, `doi:10.1007/JHEP11(2016)111`, `arXiv:1605.09242`.

[46] D. Abercrombie et al., "Dark matter benchmark models for early LHC Run-2 searches: report of the ATLAS/CMS dark matter forum", *Phys. Dark Univ.* **27** (2020) 100371, `doi:10.1016/j.dark.2019.100371`, `arXiv:1507.00966`.

[47] G. D'Ambrosio, G. F. Giudice, G. Isidori, and A. Strumia, "Minimal flavor violation: An effective field theory approach", *Nucl. Phys. B* **645** (2002) 155, `doi:10.1016/S0550-3213(02)00836-2`, `arXiv:hep-ph/0207036`.

[48] G. Isidori and D. M. Straub, "Minimal flavour violation and beyond", *Eur. Phys. J. C* **72** (2012) 2103, `doi:10.1140/epjc/s10052-012-2103-1`, `arXiv:1202.0464`.

[49] ATLAS Collaboration, "Search for dark matter produced in association with bottom or top quarks in $\sqrt{s} = 13$ TeV pp collisions with the ATLAS detector", *Eur. Phys. J. C* **78** (2018) 18, `doi:10.1140/epjc/s10052-017-5486-1`, `arXiv:1710.11412`.

[50] CMS Collaboration, "Search for dark matter particles produced in association with a top quark pair at $\sqrt{s} = 13$ TeV", *Phys. Rev. Lett.* **122** (2019) 011803, `doi:10.1103/PhysRevLett.122.011803`, `arXiv:1807.06522`.

[51] CMS Collaboration, "Search for dark matter produced in association with a single top quark or a top quark pair in proton-proton collisions at $\sqrt{s} = 13$ TeV", *JHEP* **03** (2019) 141, `doi:10.1007/JHEP03(2019)141`, `arXiv:1901.01553`.

[52] CMS Collaboration, "Search for production of four top quarks in final states with same-sign or multiple leptons in proton-proton collisions $\sqrt{s} = 13$ TeV", *Eur. Phys. J. C* **80** (2020) 75, `doi:10.1140/epjc/s10052-019-7593-7`, `arXiv:1908.06463`.

[53] CMS Collaboration, "Performance of the CMS Level-1 trigger in proton-proton collisions at $\sqrt{s} = 13$ TeV", *JINST* **15** (2020) P10017, `doi:10.1088/1748-0221/15/10/P10017`, `arXiv:2006.10165`.

[54] CMS Collaboration, "The CMS trigger system", *JINST* **12** (2017) P01020, `doi:10.1088/1748-0221/12/01/P01020`, `arXiv:1609.02366`.

[55] CMS Collaboration, "The CMS experiment at the CERN LHC", *JINST* **3** (2008) S08004, `doi:10.1088/1748-0221/3/08/S08004`.

[56] J. Alwall et al., "The automated computation of tree-level and next-to-leading order differential cross sections, and their matching to parton shower simulations", *JHEP* **07** (2014) 079, `doi:10.1007/JHEP07(2014)079`, `arXiv:1405.0301`.

[57] J. Alwall et al., "Comparative study of various algorithms for the merging of parton showers and matrix elements in hadronic collisions", *Eur. Phys. J. C* **53** (2008) 473, `doi:10.1140/epjc/s10052-007-0490-5`, `arXiv:0706.2569`.

[58] O. Mattelaer and E. Vryonidou, "Dark matter production through loop-induced processes at the LHC: the s-channel mediator case", *Eur. Phys. J. C* **75** (2015) 436, `doi:10.1140/epjc/s10052-015-3665-5`, `arXiv:1508.00564`.

[59] S. Alioli et al., "A general framework for implementing NLO calculations in shower Monte Carlo programs: the POWHEG BOX", *JHEP* **06** (2010) 043, `doi:10.1007/JHEP06(2010)043`, `arXiv:1002.2581`.

[60] S. Frixione, P. Nason, and C. Oleari, "Matching NLO QCD computations with Parton Shower simulations: the POWHEG method", *JHEP* **11** (2007) 070, `doi:10.1088/1126-6708/2007/11/070`, `arXiv:0709.2092`.

[61] P. Nason, "A new method for combining NLO QCD with shower Monte Carlo algorithms", *JHEP* **11** (2004) 040, `doi:10.1088/1126-6708/2004/11/040`, `arXiv:hep-ph/0409146`.

[62] CMS Collaboration, "Measurements of differential cross sections of top quark pair production as a function of kinematic event variables in proton-proton collisions at $\sqrt{s} = 13$ TeV", *JHEP* **06** (2018) 002, `doi:10.1007/JHEP06(2018)002`, `arXiv:1803.03991`.

[63] CMS Collaboration, "Investigations of the impact of the parton shower tuning in Pythia8 in the modelling of $t\bar{t}$ at $\sqrt{s} = 8$ and 13 TeV", CMS Physics Analysis Summary CMS-PAS-TOP-16-021, 2016.

[64] CMS Collaboration, "Extraction and validation of a new set of CMS PYTHIA8 tunes from underlying-event measurements", *Eur. Phys. J. C* **80** (2020) 4, `doi:10.1140/epjc/s10052-019-7499-4`, `arXiv:1903.12179`.

[65] E. Re, "Single-top Wt-channel production matched with parton showers using the POWHEG method", *Eur. Phys. J. C* **71** (2011) 1547, `doi:10.1140/epjc/s10052-011-1547-z`, `arXiv:1009.2450`.

[66] R. Frederix and S. Frixione, "Merging meets matching in MC@NLO", *JHEP* **12** (2012) 061, `doi:10.1007/JHEP12(2012)061`, `arXiv:1209.6215`.

[67] NNPDF Collaboration, "Parton distributions for the LHC Run II", *JHEP* **04** (2015) 040, `doi:10.1007/JHEP04(2015)040`, `arXiv:1410.8849`.

[68] NNPDF Collaboration, "Parton distributions from high-precision collider data", *Eur. Phys. J. C* **77** (2017) 663, `doi:10.1140/epjc/s10052-017-5199-5`, `arXiv:1706.00428`.

[69] T. Sjöstrand et al., "An introduction to PYTHIA 8.2", *Comput. Phys. Commun.* **191** (2015) 159, `doi:10.1016/j.cpc.2015.01.024`, `arXiv:1410.3012`.

[70] P. Skands, S. Carrazza, and J. Rojo, "Tuning PYTHIA 8.1: the Monash 2013 Tune", *Eur. Phys. J. C* **74** (2014) 3024, `doi:10.1140/epjc/s10052-014-3024-y`, `arXiv:1404.5630`.

[71] CMS Collaboration, "Event generator tunes obtained from underlying event and multiparton scattering measurements", *Eur. Phys. J. C* **76** (2016) 155, `doi:10.1140/epjc/s10052-016-3988-x`, `arXiv:1512.00815`.

[72] GEANT4 Collaboration, "GEANT4—a simulation toolkit", *Nucl. Instrum. Meth. A* **506** (2003) 250, `doi:10.1016/S0168-9002(03)01368-8`.

[73] CMS Collaboration, "The fast simulation of the CMS detector at LHC", *J. Phys. Conf. Ser.* **331** (2011) 032049, `doi:10.1088/1742-6596/331/3/032049`.

[74] A. Giammanco, "The fast simulation of the CMS experiment", *J. Phys. Conf. Ser.* **513** (2014) 022012, `doi:10.1088/1742-6596/513/2/022012`.

[75] Y. Li and F. Petriello, "Combining QCD and electroweak corrections to dilepton production in the framework of the FEWZ simulation code", *Phys. Rev. D* **86** (2012) 094034, `doi:10.1103/PhysRevD.86.094034`, `arXiv:1208.5967`.

[76] N. Kidonakis, "Theoretical results for electroweak-boson and single-top production", in *Proceedings, 23rd International Workshop on Deep-Inelastic Scattering and Related Subjects (DIS 2015): Dallas, Texas, USA, April 27-May 01, 2015*, p. 170. 2015. `arXiv:1506.04072`. [PoS(DIS2015)170]. `doi:10.22323/1.247.0170`.

[77] J. M. Campbell, R. K. Ellis, and C. Williams, "Vector boson pair production at the LHC", *JHEP* **07** (2011) 018, doi:10.1007/JHEP07(2011)018, arXiv:1105.0020.

[78] M. V. Garzelli, A. Kardos, C. G. Papadopoulos, and Z. Trocsanyi, "t$\bar{\text{t}}$W and t$\bar{\text{t}}$Z hadroproduction at NLO accuracy in QCD with parton shower and hadronization effects", *JHEP* **11** (2012) 056, doi:10.1007/JHEP11(2012)056, arXiv:1208.2665.

[79] M. Czakon, P. Fiedler, and A. Mitov, "Total top-quark pair-production cross section at hadron colliders through O(α_S^4)", *Phys. Rev. Lett.* **110** (2013) 252004, doi:10.1103/PhysRevLett.110.252004, arXiv:1303.6254.

[80] M. Czakon and A. Mitov, "Top++: A program for the calculation of the top-pair cross-section at hadron colliders", *Comput. Phys. Commun.* **185** (2014) 2930, doi:10.1016/j.cpc.2014.06.021, arXiv:1112.5675.

[81] W. Beenakker, R. Hopker, M. Spira, and P. M. Zerwas, "Squark and gluino production at hadron colliders", *Nucl. Phys. B* **492** (1997) 51, doi:10.1016/S0550-3213(97)80027-2, arXiv:hep-ph/9610490.

[82] W. Beenakker et al., "NNLL-fast: predictions for coloured supersymmetric particle production at the LHC with threshold and Coulomb resummation", *JHEP* **12** (2016) 133, doi:10.1007/JHEP12(2016)133, arXiv:1607.07741.

[83] A. Kulesza and L. Motyka, "Threshold resummation for squark-antisquark and gluino-pair production at the LHC", *Phys. Rev. Lett.* **102** (2009) 111802, doi:10.1103/PhysRevLett.102.111802, arXiv:0807.2405.

[84] A. Kulesza and L. Motyka, "Soft gluon resummation for the production of gluino-gluino and squark-antisquark pairs at the LHC", *Phys. Rev. D* **80** (2009) 095004, doi:10.1103/PhysRevD.80.095004, arXiv:0905.4749.

[85] W. Beenakker et al., "Soft-gluon resummation for squark and gluino hadroproduction", *JHEP* **12** (2009) 041, doi:10.1088/1126-6708/2009/12/041, arXiv:0909.4418.

[86] W. Beenakker et al., "Squark and gluino hadroproduction", *Int. J. Mod. Phys. A* **26** (2011) 2637, doi:10.1142/S0217751X11053560, arXiv:1105.1110.

[87] C. Borschensky et al., "Squark and gluino production cross sections in pp collisions at $\sqrt{s}$ = 13, 14, 33 and 100 TeV", *Eur. Phys. J. C* **74** (2014) 12, doi:10.1140/epjc/s10052-014-3174-y, arXiv:1407.5066.

[88] W. Beenakker et al., "NNLL resummation for squark-antisquark pair production at the LHC", *JHEP* **01** (2012) 076, doi:10.1007/JHEP01(2012)076, arXiv:1110.2446.

[89] W. Beenakker et al., "Supersymmetric top and bottom squark production at hadron colliders", *JHEP* **08** (2010) 098, doi:10.1007/JHEP08(2010)098, arXiv:1006.4771.

[90] W. Beenakker et al., "NNLL resummation for stop pair-production at the LHC", *JHEP* **05** (2016) 153, doi:10.1007/JHEP05(2016)153, arXiv:1601.02954.

[91] M. Cacciari, G. P. Salam, and G. Soyez, "The anti-k_T jet clustering algorithm", *JHEP* **04** (2008) 063, doi:10.1088/1126-6708/2008/04/063, arXiv:0802.1189.

[92] M. Cacciari, G. P. Salam, and G. Soyez, "FastJet user manual", *Eur. Phys. J. C* **72** (2012) 1896, `doi:10.1140/epjc/s10052-012-1896-2`, `arXiv:1111.6097`.

[93] CMS Collaboration, "Particle-flow reconstruction and global event description with the CMS detector", *JINST* **12** (2017) P10003, `doi:10.1088/1748-0221/12/10/P10003`, `arXiv:1706.04965`.

[94] M. Cacciari and G. P. Salam, "Pileup subtraction using jet areas", *Phys. Rev. Lett.* **659** (2008) 119, `doi:10.1016/j.physletb.2007.09.077`, `arXiv:0707.1378`.

[95] CMS Collaboration, "Jet energy scale and resolution in the CMS experiment in pp collisions at 8 TeV", *JINST* **12** (2017) P02014, `doi:10.1088/1748-0221/12/02/P02014`, `arXiv:1607.03663`.

[96] CMS Collaboration, "Jet algorithms performance in 13 TeV data", CMS Physics Analysis Summary CMS-PAS-JME-16-003, 2017.

[97] CMS Collaboration, "Identification of heavy-flavour jets with the CMS detector in pp collisions at 13 TeV", *JINST* **13** (2018) P05011, `doi:10.1088/1748-0221/13/05/P05011`, `arXiv:1712.07158`.

[98] CMS Collaboration, "Performance of the DeepJet b tagging algorithm using $41.9\,\text{fb}^{-1}$ of data from proton-proton collisions at 13 TeV with Phase 1 CMS detector", CMS Detector Performance Summary CMS-DP-2018-058, 2018.

[99] E. Bols et al., "Jet flavour classification using DeepJet", *JINST* **15** (2020) P12012, `doi:10.1088/1748-0221/15/12/P12012`, `arXiv:2008.10519`.

[100] CMS Collaboration, "Performance of missing transverse momentum reconstruction in proton-proton collisions at $\sqrt{s} = 13$ TeV using the CMS detector", *JINST* **14** (2019) P07004, `doi:10.1088/1748-0221/14/07/P07004`, `arXiv:1903.06078`.

[101] CMS Collaboration, "Reconstruction and identification of τ lepton decays to hadrons and ν_τ at CMS", *JINST* **11** (2016) P01019, `doi:10.1088/1748-0221/11/01/P01019`, `arXiv:1510.07488`.

[102] CMS Collaboration, "Performance of reconstruction and identification of tau leptons in their decays to hadrons and tau neutrino in LHC Run-2", CMS Physics Analysis Summary CMS-PAS-TAU-16-002, 2016.

[103] CMS Collaboration, "Identification of heavy, energetic, hadronically decaying particles using machine-learning techniques", *JINST* **15** (2020) P06005, `doi:10.1088/1748-0221/15/06/P06005`, `arXiv:2004.08262`.

[104] CMS Collaboration, "Search for the pair production of third-generation squarks with two-body decays to a bottom or charm quark and a neutralino in proton–proton collisions at $\sqrt{s} = 13$ TeV", *Phys. Lett. B* **778** (2018) 263, `doi:10.1016/j.physletb.2018.01.012`, `arXiv:1707.07274`.

[105] CMS Collaboration, "Performance of electron reconstruction and selection with the CMS detector in proton-proton collisions at $\sqrt{s} = 8$ TeV", *JINST* **10** (2015) P06005, `doi:10.1088/1748-0221/10/06/P06005`, `arXiv:1502.02701`.

[106] M. Abadi et al., "TensorFlow: Large-scale machine learning on heterogeneous systems", 2016. `arXiv:1603.04467`. Software available from `https://www.tensorflow.org/`.

[107] F. Chollet et al., "Keras", 2015. Software available from `https://keras.io`.

[108] D. P. Kingma and J. Ba, "Adam: A method for stochastic optimization", 2014. `arXiv:1412.6980`. Software available from `https://keras.io/api/optimizers/adam/`.

[109] CMS Collaboration, "Performance of the CMS muon detector and muon reconstruction with proton-proton collisions at $\sqrt{s} = 13$ TeV", *JINST* **13** (2018) P06015, `doi:10.1088/1748-0221/13/06/P06015`, `arXiv:1804.04528`.

[110] CMS Collaboration, "Performance of photon reconstruction and identification with the CMS detector in proton-proton collisions at $\sqrt{s} = 8$ TeV", *JINST* **10** (2015) P08010, `doi:10.1088/1748-0221/10/08/P08010`, `arXiv:1502.02702`.

[111] CMS Collaboration, "Description and performance of track and primary-vertex reconstruction with the CMS tracker", *JINST* **9** (2014) P10009, `doi:10.1088/1748-0221/9/10/P10009`, `arXiv:1405.6569`.

[112] CMS Collaboration, "Measurement of the inelastic proton-proton cross section at $\sqrt{s} = 13$ TeV", *JHEP* **07** (2018) 161, `doi:10.1007/JHEP07(2018)161`, `arXiv:1802.02613`.

[113] J. Butterworth et al., "PDF4LHC recommendations for LHC Run II", *J. Phys. G* **43** (2016) 023001, `doi:10.1088/0954-3899/43/2/023001`, `arXiv:1510.03865`.

[114] CMS Collaboration, "Measurement of the top quark mass using proton-proton data at $\sqrt{s} = 7$ and 8 TeV", *Phys. Rev. D* **93** (2016) 072004, `doi:10.1103/PhysRevD.93.072004`, `arXiv:1509.04044`.

[115] CMS Collaboration, "Precision luminosity measurement in proton-proton collisions at $\sqrt{s} = 13$ TeV in 2015 and 2016 at CMS", 2021. `arXiv:2104.01927`. Submitted to Eur. Phys. J. C.

[116] CMS Collaboration, "CMS luminosity measurements for the 2016 data-taking period", CMS Physics Analysis Summary CMS-PAS-LUMI-17-001, 2017.

[117] CMS Collaboration, "CMS luminosity measurements for the 2017 data-taking period", CMS Physics Analysis Summary CMS-PAS-LUMI-17-004, 2017.

[118] CMS Collaboration, "CMS luminosity measurements for the 2018 data-taking period at $\sqrt{s} = 13$ TeV", CMS Physics Analysis Summary CMS-PAS-LUMI-18-002, 2019.

[119] R. Barlow and C. Beeston, "Fitting using finite Monte Carlo samples", *Comput. Phys. Commun.* **77** (1993) 219, `doi:10.1016/0010-4655(93)90005-W`.

[120] G. Cowan, K. Cranmer, E. Gross, and O. Vitells, "Asymptotic formulae for likelihood-based tests of new physics", *Eur. Phys. J. C* **71** (2011) 1554, `doi:10.1140/epjc/s10052-011-1554-0`, `arXiv:1007.1727`. [Erratum: `doi:10.1140/epjc/s10052-013-2501-z`].

[121] T. Junk, "Confidence level computation for combining searches with small statistics", *Nucl. Instrum. Meth. A* **434** (1999) 435, `doi:10.1016/S0168-9002(99)00498-2`, `arXiv:hep-ex/9902006`.

[122] A. L. Read, "Presentation of search results: the CL$_s$ technique", in *Durham IPPP Workshop: Advanced Statistical Techniques in Particle Physics*, p. 2693. Durham, UK, March, 2002. [J. Phys. G 28 (2002) 2693]. `doi:10.1088/0954-3899/28/10/313`.

[123] The ATLAS Collaboration, The CMS Collaboration, The LHC Higgs Combination Group, "Procedure for the LHC Higgs boson search combination in Summer 2011", Technical Report CMS-NOTE-2011-005, ATL-PHYS-PUB-2011-11, 2011.

A The CMS Collaboration

Yerevan Physics Institute, Yerevan, Armenia
A. Tumasyan

Institut für Hochenergiephysik, Wien, Austria
W. Adam, J.W. Andrejkovic, T. Bergauer, S. Chatterjee, M. Dragicevic, A. Escalante Del Valle, R. Frühwirth[1], M. Jeitler[1], N. Krammer, L. Lechner, D. Liko, I. Mikulec, P. Paulitsch, F.M. Pitters, J. Schieck[1], R. Schöfbeck, M. Spanring, S. Templ, W. Waltenberger, C.-E. Wulz[1]

Institute for Nuclear Problems, Minsk, Belarus
V. Chekhovsky, A. Litomin, V. Makarenko

Universiteit Antwerpen, Antwerpen, Belgium
M.R. Darwish[2], E.A. De Wolf, X. Janssen, T. Kello[3], A. Lelek, H. Rejeb Sfar, P. Van Mechelen, S. Van Putte, N. Van Remortel

Vrije Universiteit Brussel, Brussel, Belgium
F. Blekman, E.S. Bols, J. D'Hondt, J. De Clercq, M. Delcourt, H. El Faham, S. Lowette, S. Moortgat, A. Morton, D. Müller, A.R. Sahasransu, S. Tavernier, W. Van Doninck, P. Van Mulders

Université Libre de Bruxelles, Bruxelles, Belgium
D. Beghin, B. Bilin, B. Clerbaux, G. De Lentdecker, L. Favart, A. Grebenyuk, A.K. Kalsi, K. Lee, M. Mahdavikhorrami, I. Makarenko, L. Moureaux, L. Pétré, A. Popov, N. Postiau, E. Starling, L. Thomas, M. Vanden Bemden, C. Vander Velde, P. Vanlaer, D. Vannerom, L. Wezenbeek

Ghent University, Ghent, Belgium
T. Cornelis, D. Dobur, J. Knolle, L. Lambrecht, G. Mestdach, M. Niedziela, C. Roskas, A. Samalan, K. Skovpen, M. Tytgat, W. Verbeke, B. Vermassen, M. Vit

Université Catholique de Louvain, Louvain-la-Neuve, Belgium
A. Bethani, G. Bruno, F. Bury, C. Caputo, P. David, C. Delaere, I.S. Donertas, A. Giammanco, K. Jaffel, Sa. Jain, V. Lemaitre, K. Mondal, J. Prisciandaro, A. Taliercio, M. Teklishyn, T.T. Tran, P. Vischia, S. Wertz

Centro Brasileiro de Pesquisas Fisicas, Rio de Janeiro, Brazil
G.A. Alves, C. Hensel, A. Moraes

Universidade do Estado do Rio de Janeiro, Rio de Janeiro, Brazil
W.L. Aldá Júnior, M. Alves Gallo Pereira, M. Barroso Ferreira Filho, H. Brandao Malbouisson, W. Carvalho, J. Chinellato[4], E.M. Da Costa, G.G. Da Silveira[5], D. De Jesus Damiao, S. Fonseca De Souza, D. Matos Figueiredo, C. Mora Herrera, K. Mota Amarilo, L. Mundim, H. Nogima, P. Rebello Teles, A. Santoro, S.M. Silva Do Amaral, A. Sznajder, M. Thiel, F. Torres Da Silva De Araujo, A. Vilela Pereira

Universidade Estadual Paulista [a], Universidade Federal do ABC [b], São Paulo, Brazil
C.A. Bernardes[a,a,5], L. Calligaris[a], T.R. Fernandez Perez Tomei[a], E.M. Gregores[a,b], D.S. Lemos[a], P.G. Mercadante[a,b], S.F. Novaes[a], Sandra S. Padula[a]

Institute for Nuclear Research and Nuclear Energy, Bulgarian Academy of Sciences, Sofia, Bulgaria
A. Aleksandrov, G. Antchev, R. Hadjiiska, P. Iaydjiev, M. Misheva, M. Rodozov, M. Shopova, G. Sultanov

University of Sofia, Sofia, Bulgaria
A. Dimitrov, T. Ivanov, L. Litov, B. Pavlov, P. Petkov, A. Petrov

Beihang University, Beijing, China
T. Cheng, Q. Guo, T. Javaid[6], M. Mittal, H. Wang, L. Yuan

Department of Physics, Tsinghua University, Beijing, China
M. Ahmad, G. Bauer, C. Dozen[7], Z. Hu, J. Martins[8], Y. Wang, K. Yi[9,10]

Institute of High Energy Physics, Beijing, China
E. Chapon, G.M. Chen[6], H.S. Chen[6], M. Chen, F. Iemmi, A. Kapoor, D. Leggat, H. Liao, Z.-A. LIU[6], V. Milosevic, F. Monti, R. Sharma, J. Tao, J. Thomas-wilsker, J. Wang, H. Zhang, S. Zhang[6], J. Zhao

State Key Laboratory of Nuclear Physics and Technology, Peking University, Beijing, China
A. Agapitos, Y. An, Y. Ban, C. Chen, A. Levin, Q. Li, X. Lyu, Y. Mao, S.J. Qian, D. Wang, Q. Wang, J. Xiao

Sun Yat-Sen University, Guangzhou, China
M. Lu, Z. You

Institute of Modern Physics and Key Laboratory of Nuclear Physics and Ion-beam Application (MOE) - Fudan University, Shanghai, China
X. Gao[3], H. Okawa

Zhejiang University, Hangzhou, China
Z. Lin, M. Xiao

Universidad de Los Andes, Bogota, Colombia
C. Avila, A. Cabrera, C. Florez, J. Fraga, A. Sarkar, M.A. Segura Delgado

Universidad de Antioquia, Medellin, Colombia
J. Mejia Guisao, F. Ramirez, J.D. Ruiz Alvarez, C.A. Salazar González

University of Split, Faculty of Electrical Engineering, Mechanical Engineering and Naval Architecture, Split, Croatia
D. Giljanovic, N. Godinovic, D. Lelas, I. Puljak

University of Split, Faculty of Science, Split, Croatia
Z. Antunovic, M. Kovac, T. Sculac

Institute Rudjer Boskovic, Zagreb, Croatia
V. Brigljevic, D. Ferencek, D. Majumder, M. Roguljic, A. Starodumov[11], T. Susa

University of Cyprus, Nicosia, Cyprus
A. Attikis, K. Christoforou, E. Erodotou, A. Ioannou, G. Kole, M. Kolosova, S. Konstantinou, J. Mousa, C. Nicolaou, F. Ptochos, P.A. Razis, H. Rykaczewski, H. Saka

Charles University, Prague, Czech Republic
M. Finger[12], M. Finger Jr.[12], A. Kveton

Escuela Politecnica Nacional, Quito, Ecuador
E. Ayala

Universidad San Francisco de Quito, Quito, Ecuador
E. Carrera Jarrin

Academy of Scientific Research and Technology of the Arab Republic of Egypt, Egyptian Network of High Energy Physics, Cairo, Egypt
H. Abdalla[13], E. Salama[14,15]

Center for High Energy Physics (CHEP-FU), Fayoum University, El-Fayoum, Egypt
A. Lotfy, M.A. Mahmoud

National Institute of Chemical Physics and Biophysics, Tallinn, Estonia
S. Bhowmik, R.K. Dewanjee, K. Ehataht, M. Kadastik, S. Nandan, C. Nielsen, J. Pata, M. Raidal, L. Tani, C. Veelken

Department of Physics, University of Helsinki, Helsinki, Finland
P. Eerola, L. Forthomme, H. Kirschenmann, K. Osterberg, M. Voutilainen

Helsinki Institute of Physics, Helsinki, Finland
S. Bharthuar, E. Brücken, F. Garcia, J. Havukainen, M.S. Kim, R. Kinnunen, T. Lampén, K. Lassila-Perini, S. Lehti, T. Lindén, M. Lotti, L. Martikainen, M. Myllymäki, J. Ott, H. Siikonen, E. Tuominen, J. Tuominiemi

Lappeenranta University of Technology, Lappeenranta, Finland
P. Luukka, H. Petrow, T. Tuuva

IRFU, CEA, Université Paris-Saclay, Gif-sur-Yvette, France
C. Amendola, M. Besancon, F. Couderc, M. Dejardin, D. Denegri, J.L. Faure, F. Ferri, S. Ganjour, A. Givernaud, P. Gras, G. Hamel de Monchenault, P. Jarry, B. Lenzi, E. Locci, J. Malcles, J. Rander, A. Rosowsky, M.Ö. Sahin, A. Savoy-Navarro[16], M. Titov, G.B. Yu

Laboratoire Leprince-Ringuet, CNRS/IN2P3, Ecole Polytechnique, Institut Polytechnique de Paris, Palaiseau, France
S. Ahuja, F. Beaudette, M. Bonanomi, A. Buchot Perraguin, P. Busson, A. Cappati, C. Charlot, O. Davignon, B. Diab, G. Falmagne, S. Ghosh, R. Granier de Cassagnac, A. Hakimi, I. Kucher, J. Motta, M. Nguyen, C. Ochando, P. Paganini, J. Rembser, R. Salerno, J.B. Sauvan, Y. Sirois, A. Tarabini, A. Zabi, A. Zghiche

Université de Strasbourg, CNRS, IPHC UMR 7178, Strasbourg, France
J.-L. Agram[17], J. Andrea, D. Apparu, D. Bloch, G. Bourgatte, J.-M. Brom, E.C. Chabert, C. Collard, D. Darej, J.-C. Fontaine[17], U. Goerlach, C. Grimault, A.-C. Le Bihan, E. Nibigira, P. Van Hove

Institut de Physique des 2 Infinis de Lyon (IP2I), Villeurbanne, France
E. Asilar, S. Beauceron, C. Bernet, G. Boudoul, C. Camen, A. Carle, N. Chanon, D. Contardo, P. Depasse, H. El Mamouni, J. Fay, S. Gascon, M. Gouzevitch, B. Ille, I.B. Laktineh, H. Lattaud, A. Lesauvage, M. Lethuillier, L. Mirabito, S. Perries, K. Shchablo, V. Sordini, L. Torterotot, G. Touquet, M. Vander Donckt, S. Viret

Georgian Technical University, Tbilisi, Georgia
G. Adamov, I. Lomidze, Z. Tsamalaidze[12]

RWTH Aachen University, I. Physikalisches Institut, Aachen, Germany
L. Feld, K. Klein, M. Lipinski, D. Meuser, A. Pauls, M.P. Rauch, N. Röwert, J. Schulz, M. Teroerde

RWTH Aachen University, III. Physikalisches Institut A, Aachen, Germany
A. Dodonova, D. Eliseev, M. Erdmann, P. Fackeldey, B. Fischer, S. Ghosh, T. Hebbeker, K. Hoepfner, F. Ivone, H. Keller, L. Mastrolorenzo, M. Merschmeyer, A. Meyer, G. Mocellin,

S. Mondal, S. Mukherjee, D. Noll, A. Novak, T. Pook, A. Pozdnyakov, Y. Rath, H. Reithler, J. Roemer, A. Schmidt, S.C. Schuler, A. Sharma, L. Vigilante, S. Wiedenbeck, S. Zaleski

RWTH Aachen University, III. Physikalisches Institut B, Aachen, Germany
C. Dziwok, G. Flügge, W. Haj Ahmad[18], O. Hlushchenko, T. Kress, A. Nowack, C. Pistone, O. Pooth, D. Roy, H. Sert, A. Stahl[19], T. Ziemons

Deutsches Elektronen-Synchrotron, Hamburg, Germany
H. Aarup Petersen, M. Aldaya Martin, P. Asmuss, I. Babounikau, S. Baxter, O. Behnke, A. Bermúdez Martínez, S. Bhattacharya, A.A. Bin Anuar, K. Borras[20], V. Botta, D. Brunner, A. Campbell, A. Cardini, C. Cheng, F. Colombina, S. Consuegra Rodríguez, G. Correia Silva, V. Danilov, L. Didukh, G. Eckerlin, D. Eckstein, L.I. Estevez Banos, O. Filatov, E. Gallo[21], A. Geiser, A. Giraldi, A. Grohsjean, M. Guthoff, A. Jafari[22], N.Z. Jomhari, H. Jung, A. Kasem[20], M. Kasemann, H. Kaveh, C. Kleinwort, D. Krücker, W. Lange, J. Lidrych, K. Lipka, W. Lohmann[23], R. Mankel, I.-A. Melzer-Pellmann, J. Metwally, A.B. Meyer, M. Meyer, J. Mnich, A. Mussgiller, Y. Otarid, D. Pérez Adán, D. Pitzl, A. Raspereza, B. Ribeiro Lopes, J. Rübenach, A. Saggio, A. Saibel, M. Savitskyi, M. Scham, V. Scheurer, C. Schwanenberger[21], A. Singh, R.E. Sosa Ricardo, D. Stafford, N. Tonon, O. Turkot, M. Van De Klundert, R. Walsh, D. Walter, Y. Wen, K. Wichmann, L. Wiens, C. Wissing, S. Wuchterl

University of Hamburg, Hamburg, Germany
R. Aggleton, S. Albrecht, S. Bein, L. Benato, A. Benecke, P. Connor, K. De Leo, M. Eich, F. Feindt, A. Fröhlich, C. Garbers, E. Garutti, P. Gunnellini, J. Haller, A. Hinzmann, G. Kasieczka, R. Klanner, R. Kogler, T. Kramer, V. Kutzner, J. Lange, T. Lange, A. Lobanov, A. Malara, A. Nigamova, K.J. Pena Rodriguez, O. Rieger, P. Schleper, M. Schröder, J. Schwandt, D. Schwarz, J. Sonneveld, H. Stadie, G. Steinbrück, A. Tews, B. Vormwald, I. Zoi

Karlsruher Institut fuer Technologie, Karlsruhe, Germany
J. Bechtel, T. Berger, E. Butz, R. Caspart, T. Chwalek, W. De Boer[†], A. Dierlamm, A. Droll, K. El Morabit, N. Faltermann, M. Giffels, J.o. Gosewisch, A. Gottmann, F. Hartmann[19], C. Heidecker, U. Husemann, I. Katkov[24], P. Keicher, R. Koppenhöfer, S. Maier, M. Metzler, S. Mitra, Th. Müller, M. Neukum, A. Nürnberg, G. Quast, K. Rabbertz, J. Rauser, D. Savoiu, M. Schnepf, D. Seith, I. Shvetsov, H.J. Simonis, R. Ulrich, J. Van Der Linden, R.F. Von Cube, M. Wassmer, M. Weber, S. Wieland, R. Wolf, S. Wozniewski, S. Wunsch

Institute of Nuclear and Particle Physics (INPP), NCSR Demokritos, Aghia Paraskevi, Greece
G. Anagnostou, G. Daskalakis, T. Geralis, A. Kyriakis, D. Loukas, A. Stakia

National and Kapodistrian University of Athens, Athens, Greece
M. Diamantopoulou, D. Karasavvas, G. Karathanasis, P. Kontaxakis, C.K. Koraka, A. Manousakis-katsikakis, A. Panagiotou, I. Papavergou, N. Saoulidou, K. Theofilatos, E. Tziaferi, K. Vellidis, E. Vourliotis

National Technical University of Athens, Athens, Greece
G. Bakas, K. Kousouris, I. Papakrivopoulos, G. Tsipolitis, A. Zacharopoulou

University of Ioánnina, Ioánnina, Greece
I. Evangelou, C. Foudas, P. Gianneios, P. Katsoulis, P. Kokkas, N. Manthos, I. Papadopoulos, J. Strologas

MTA-ELTE Lendület CMS Particle and Nuclear Physics Group, Eötvös Loránd University,

Budapest, Hungary
M. Csanad, K. Farkas, M.M.A. Gadallah[25], S. Lökös[26], P. Major, K. Mandal, A. Mehta, G. Pasztor, A.J. Rádl, O. Surányi, G.I. Veres

Wigner Research Centre for Physics, Budapest, Hungary
M. Bartók[27], G. Bencze, C. Hajdu, D. Horvath[28], F. Sikler, V. Veszpremi, G. Vesztergombi[†]

Institute of Nuclear Research ATOMKI, Debrecen, Hungary
S. Czellar, J. Karancsi[27], J. Molnar, Z. Szillasi, D. Teyssier

Institute of Physics, University of Debrecen, Debrecen, Hungary
P. Raics, Z.L. Trocsanyi[29], B. Ujvari

Karoly Robert Campus, MATE Institute of Technology
T. Csorgo[30], F. Nemes[30], T. Novak

Indian Institute of Science (IISc), Bangalore, India
J.R. Komaragiri, D. Kumar, L. Panwar, P.C. Tiwari

National Institute of Science Education and Research, HBNI, Bhubaneswar, India
S. Bahinipati[31], C. Kar, P. Mal, T. Mishra, V.K. Muraleedharan Nair Bindhu[32], A. Nayak[32], P. Saha, N. Sur, S.K. Swain, D. Vats[32]

Panjab University, Chandigarh, India
S. Bansal, S.B. Beri, V. Bhatnagar, G. Chaudhary, S. Chauhan, N. Dhingra[33], R. Gupta, A. Kaur, M. Kaur, S. Kaur, P. Kumari, M. Meena, K. Sandeep, J.B. Singh, A.K. Virdi

University of Delhi, Delhi, India
A. Ahmed, A. Bhardwaj, B.C. Choudhary, M. Gola, S. Keshri, A. Kumar, M. Naimuddin, P. Priyanka, K. Ranjan, A. Shah

Saha Institute of Nuclear Physics, HBNI, Kolkata, India
M. Bharti[34], R. Bhattacharya, S. Bhattacharya, D. Bhowmik, S. Dutta, S. Dutta, B. Gomber[35], M. Maity[36], P. Palit, P.K. Rout, G. Saha, B. Sahu, S. Sarkar, M. Sharan, B. Singh[34], S. Thakur[34]

Indian Institute of Technology Madras, Madras, India
P.K. Behera, S.C. Behera, P. Kalbhor, A. Muhammad, R. Pradhan, P.R. Pujahari, A. Sharma, A.K. Sikdar

Bhabha Atomic Research Centre, Mumbai, India
D. Dutta, V. Jha, V. Kumar, D.K. Mishra, K. Naskar[37], P.K. Netrakanti, L.M. Pant, P. Shukla

Tata Institute of Fundamental Research-A, Mumbai, India
T. Aziz, S. Dugad, M. Kumar, U. Sarkar

Tata Institute of Fundamental Research-B, Mumbai, India
S. Banerjee, R. Chudasama, M. Guchait, S. Karmakar, S. Kumar, G. Majumder, K. Mazumdar, S. Mukherjee

Indian Institute of Science Education and Research (IISER), Pune, India
K. Alpana, S. Dube, B. Kansal, A. Laha, S. Pandey, A. Rane, A. Rastogi, S. Sharma

Department of Physics, Isfahan University of Technology, Isfahan, Iran
H. Bakhshiansohi[38], M. Zeinali[39]

Institute for Research in Fundamental Sciences (IPM), Tehran, Iran
S. Chenarani[40], S.M. Etesami, M. Khakzad, M. Mohammadi Najafabadi

University College Dublin, Dublin, Ireland
M. Grunewald

INFN Sezione di Bari ^{a}, Università di Bari ^{b}, Politecnico di Bari ^{c}, Bari, Italy
M. Abbrescia^{a,b}, R. Aly^{a,b,41}, C. Aruta^{a,b}, A. Colaleo^a, D. Creanza^{a,c}, N. De Filippis^{a,c}, M. De Palma^{a,b}, A. Di Florio^{a,b}, A. Di Pilato^{a,b}, W. Elmetenawee^{a,b}, L. Fiore^a, A. Gelmi^{a,b}, M. Gul^a, G. Iaselli^{a,c}, M. Ince^{a,b}, S. Lezki^{a,b}, G. Maggi^{a,c}, M. Maggi^a, I. Margjeka^{a,b}, V. Mastrapasqua^{a,b}, J.A. Merlin^a, S. My^{a,b}, S. Nuzzo^{a,b}, A. Pellecchia^{a,b}, A. Pompili^{a,b}, G. Pugliese^{a,c}, A. Ranieri^a, G. Selvaggi^{a,b}, L. Silvestris^a, F.M. Simone^{a,b}, R. Venditti^a, P. Verwilligen^a

INFN Sezione di Bologna ^{a}, Università di Bologna ^{b}, Bologna, Italy
G. Abbiendi^a, C. Battilana^{a,b}, D. Bonacorsi^{a,b}, L. Borgonovi^a, L. Brigliadori^a, R. Campanini^{a,b}, P. Capiluppi^{a,b}, A. Castro^{a,b}, F.R. Cavallo^a, M. Cuffiani^{a,b}, G.M. Dallavalle^a, T. Diotalevi^{a,b}, F. Fabbri^a, A. Fanfani^{a,b}, P. Giacomelli^a, L. Giommi^{a,b}, C. Grandi^a, L. Guiducci^{a,b}, S. Lo Meo^{a,42}, L. Lunerti^{a,b}, S. Marcellini^a, G. Masetti^a, F.L. Navarria^{a,b}, A. Perrotta^a, F. Primavera^{a,b}, A.M. Rossi^{a,b}, T. Rovelli^{a,b}, G.P. Siroli^{a,b}

INFN Sezione di Catania ^{a}, Università di Catania ^{b}, Catania, Italy
S. Albergo^{a,b,43}, S. Costa^{a,b,43}, A. Di Mattia^a, R. Potenza^{a,b}, A. Tricomi^{a,b,43}, C. Tuve^{a,b}

INFN Sezione di Firenze ^{a}, Università di Firenze ^{b}, Firenze, Italy
G. Barbagli^a, A. Cassese^a, R. Ceccarelli^{a,b}, V. Ciulli^{a,b}, C. Civinini^a, R. D'Alessandro^{a,b}, E. Focardi^{a,b}, G. Latino^{a,b}, P. Lenzi^{a,b}, M. Lizzo^{a,b}, M. Meschini^a, S. Paoletti^a, R. Seidita^{a,b}, G. Sguazzoni^a, L. Viliani^a

INFN Laboratori Nazionali di Frascati, Frascati, Italy
L. Benussi, S. Bianco, D. Piccolo

INFN Sezione di Genova ^{a}, Università di Genova ^{b}, Genova, Italy
M. Bozzo^{a,b}, F. Ferro^a, R. Mulargia^{a,b}, E. Robutti^a, S. Tosi^{a,b}

INFN Sezione di Milano-Bicocca ^{a}, Università di Milano-Bicocca ^{b}, Milano, Italy
A. Benaglia^a, F. Brivio^{a,b}, F. Cetorelli^{a,b}, V. Ciriolo^{a,b,19}, F. De Guio^{a,b}, M.E. Dinardo^{a,b}, P. Dini^a, S. Gennai^a, A. Ghezzi^{a,b}, P. Govoni^{a,b}, L. Guzzi^{a,b}, M. Malberti^a, S. Malvezzi^a, A. Massironi^a, D. Menasce^a, L. Moroni^a, M. Paganoni^{a,b}, D. Pedrini^a, S. Ragazzi^{a,b}, N. Redaelli^a, T. Tabarelli de Fatis^{a,b}, D. Valsecchi^{a,b,19}, D. Zuolo^{a,b}

INFN Sezione di Napoli ^{a}, Università di Napoli 'Federico II' ^{b}, Napoli, Italy, Università della Basilicata ^{c}, Potenza, Italy, Università G. Marconi ^{d}, Roma, Italy
S. Buontempo^a, F. Carnevali^{a,b}, N. Cavallo^{a,c}, A. De Iorio^{a,b}, F. Fabozzi^{a,c}, A.O.M. Iorio^{a,b}, L. Lista^{a,b}, S. Meola^{a,d,19}, P. Paolucci^{a,19}, B. Rossi^a, C. Sciacca^{a,b}

INFN Sezione di Padova ^{a}, Università di Padova ^{b}, Padova, Italy, Università di Trento ^{c}, Trento, Italy
P. Azzi^a, N. Bacchetta^a, D. Bisello^{a,b}, P. Bortignon^a, A. Bragagnolo^{a,b}, R. Carlin^{a,b}, P. Checchia^a, T. Dorigo^a, U. Dosselli^a, F. Gasparini^{a,b}, U. Gasparini^{a,b}, S.Y. Hoh^{a,b}, L. Layer^{a,44}, M. Margoni^{a,b}, A.T. Meneguzzo^{a,b}, J. Pazzini^{a,b}, M. Presilla^{a,b}, P. Ronchese^{a,b}, R. Rossin^{a,b}, F. Simonetto^{a,b}, G. Strong^a, M. Tosi^{a,b}, H. YARAR^{a,b}, M. Zanetti^{a,b}, P. Zotto^{a,b}, A. Zucchetta^{a,b}, G. Zumerle^{a,b}

INFN Sezione di Pavia ^{a}, Università di Pavia ^{b}, Pavia, Italy
C. Aime'^{a,b}, A. Braghieri^a, S. Calzaferri^{a,b}, D. Fiorina^{a,b}, P. Montagna^{a,b}, S.P. Ratti^{a,b}, V. Re^a, C. Riccardi^{a,b}, P. Salvini^a, I. Vai^a, P. Vitulo^{a,b}

INFN Sezione di Perugia ^{a}, Università di Perugia ^{b}, Perugia, Italy
P. Asenov^{a,45}, G.M. Bilei^a, D. Ciangottini^{a,b}, L. Fanò^{a,b}, P. Lariccia^{a,b}, M. Magherini^b, G. Mantovani^{a,b}, V. Mariani^{a,b}, M. Menichelli^a, F. Moscatelli^{a,45}, A. Piccinelli^{a,b}, A. Rossi^{a,b}, A. Santocchia^{a,b}, D. Spiga^a, T. Tedeschi^{a,b}

INFN Sezione di Pisa ^{a}, Università di Pisa ^{b}, Scuola Normale Superiore di Pisa ^{c}, Pisa Italy, Università di Siena ^{d}, Siena, Italy
P. Azzurri^a, G. Bagliesi^a, V. Bertacchi^{a,c}, L. Bianchini^a, T. Boccali^a, E. Bossini^{a,b}, R. Castaldi^a, M.A. Ciocci^{a,b}, V. D'Amante^{a,d}, R. Dell'Orso^a, M.R. Di Domenico^{a,d}, S. Donato^a, A. Giassi^a, F. Ligabue^{a,c}, E. Manca^{a,c}, G. Mandorli^{a,c}, A. Messineo^{a,b}, F. Palla^a, S. Parolia^{a,b}, G. Ramirez-Sanchez^{a,c}, A. Rizzi^{a,b}, G. Rolandi^{a,c}, S. Roy Chowdhury^{a,c}, A. Scribano^a, N. Shafiei^{a,b}, P. Spagnolo^a, R. Tenchini^a, G. Tonelli^{a,b}, N. Turini^{a,d}, A. Venturi^a, P.G. Verdini^a

INFN Sezione di Roma ^{a}, Sapienza Università di Roma ^{b}, Rome, Italy
M. Campana^{a,b}, F. Cavallari^a, D. Del Re^{a,b}, E. Di Marco^a, M. Diemoz^a, E. Longo^{a,b}, P. Meridiani^a, G. Organtini^{a,b}, F. Pandolfi^a, R. Paramatti^{a,b}, C. Quaranta^{a,b}, S. Rahatlou^{a,b}, C. Rovelli^a, F. Santanastasio^{a,b}, L. Soffi^a, R. Tramontano^{a,b}

INFN Sezione di Torino ^{a}, Università di Torino ^{b}, Torino, Italy, Università del Piemonte Orientale ^{c}, Novara, Italy
N. Amapane^{a,b}, R. Arcidiacono^{a,c}, S. Argiro^{a,b}, M. Arneodo^{a,c}, N. Bartosik^a, R. Bellan^{a,b}, A. Bellora^{a,b}, J. Berenguer Antequera^{a,b}, C. Biino^a, N. Cartiglia^a, S. Cometti^a, M. Costa^{a,b}, R. Covarelli^{a,b}, N. Demaria^a, B. Kiani^{a,b}, F. Legger^a, C. Mariotti^a, S. Maselli^a, E. Migliore^{a,b}, E. Monteil^{a,b}, M. Monteno^a, M.M. Obertino^{a,b}, G. Ortona^a, L. Pacher^{a,b}, N. Pastrone^a, M. Pelliccioni^a, G.L. Pinna Angioni^{a,b}, M. Ruspa^{a,c}, K. Shchelina^{a,b}, F. Siviero^{a,b}, V. Sola^a, A. Solano^{a,b}, D. Soldi^{a,b}, A. Staiano^a, M. Tornago^{a,b}, D. Trocino^{a,b}, A. Vagnerini

INFN Sezione di Trieste ^{a}, Università di Trieste ^{b}, Trieste, Italy
S. Belforte^a, V. Candelise^{a,b}, M. Casarsa^a, F. Cossutti^a, A. Da Rold^{a,b}, G. Della Ricca^{a,b}, G. Sorrentino^{a,b}, F. Vazzoler^{a,b}

Kyungpook National University, Daegu, Korea
S. Dogra, C. Huh, B. Kim, D.H. Kim, G.N. Kim, J. Kim, J. Lee, S.W. Lee, C.S. Moon, Y.D. Oh, S.I. Pak, B.C. Radburn-Smith, S. Sekmen, Y.C. Yang

Chonnam National University, Institute for Universe and Elementary Particles, Kwangju, Korea
H. Kim, D.H. Moon

Hanyang University, Seoul, Korea
B. Francois, T.J. Kim, J. Park

Korea University, Seoul, Korea
S. Cho, S. Choi, Y. Go, B. Hong, K. Lee, K.S. Lee, J. Lim, J. Park, S.K. Park, J. Yoo

Kyung Hee University, Department of Physics, Seoul, Republic of Korea
J. Goh, A. Gurtu

Sejong University, Seoul, Korea
H.S. Kim, Y. Kim

Seoul National University, Seoul, Korea
J. Almond, J.H. Bhyun, J. Choi, S. Jeon, J. Kim, J.S. Kim, S. Ko, H. Kwon, H. Lee, S. Lee, B.H. Oh, M. Oh, S.B. Oh, H. Seo, U.K. Yang, I. Yoon

University of Seoul, Seoul, Korea
W. Jang, D. Jeon, D.Y. Kang, Y. Kang, J.H. Kim, S. Kim, B. Ko, J.S.H. Lee, Y. Lee, I.C. Park, Y. Roh, M.S. Ryu, D. Song, I.J. Watson, S. Yang

Yonsei University, Department of Physics, Seoul, Korea
S. Ha, H.D. Yoo

Sungkyunkwan University, Suwon, Korea
M. Choi, Y. Jeong, H. Lee, Y. Lee, I. Yu

College of Engineering and Technology, American University of the Middle East (AUM), Egaila, Kuwait
T. Beyrouthy, Y. Maghrbi

Riga Technical University, Riga, Latvia
T. Torims, V. Veckalns[46]

Vilnius University, Vilnius, Lithuania
M. Ambrozas, A. Carvalho Antunes De Oliveira, A. Juodagalvis, A. Rinkevicius, G. Tamulaitis

National Centre for Particle Physics, Universiti Malaya, Kuala Lumpur, Malaysia
N. Bin Norjoharuddeen, W.A.T. Wan Abdullah, M.N. Yusli, Z. Zolkapli

Universidad de Sonora (UNISON), Hermosillo, Mexico
J.F. Benitez, A. Castaneda Hernandez, M. León Coello, J.A. Murillo Quijada, A. Sehrawat, L. Valencia Palomo

Centro de Investigacion y de Estudios Avanzados del IPN, Mexico City, Mexico
G. Ayala, H. Castilla-Valdez, E. De La Cruz-Burelo, I. Heredia-De La Cruz[47], R. Lopez-Fernandez, C.A. Mondragon Herrera, D.A. Perez Navarro, A. Sanchez-Hernandez

Universidad Iberoamericana, Mexico City, Mexico
S. Carrillo Moreno, C. Oropeza Barrera, M. Ramirez-Garcia, F. Vazquez Valencia

Benemerita Universidad Autonoma de Puebla, Puebla, Mexico
I. Pedraza, H.A. Salazar Ibarguen, C. Uribe Estrada

University of Montenegro, Podgorica, Montenegro
J. Mijuskovic[48], N. Raicevic

University of Auckland, Auckland, New Zealand
D. Krofcheck

University of Canterbury, Christchurch, New Zealand
S. Bheesette, P.H. Butler

National Centre for Physics, Quaid-I-Azam University, Islamabad, Pakistan
A. Ahmad, M.I. Asghar, A. Awais, M.I.M. Awan, H.R. Hoorani, W.A. Khan, M.A. Shah, M. Shoaib, M. Waqas

AGH University of Science and Technology Faculty of Computer Science, Electronics and Telecommunications, Krakow, Poland
V. Avati, L. Grzanka, M. Malawski

National Centre for Nuclear Research, Swierk, Poland
H. Bialkowska, M. Bluj, B. Boimska, M. Górski, M. Kazana, M. Szleper, P. Zalewski

Institute of Experimental Physics, Faculty of Physics, University of Warsaw, Warsaw, Poland
K. Bunkowski, K. Doroba, A. Kalinowski, M. Konecki, J. Krolikowski, M. Walczak

Laboratório de Instrumentação e Física Experimental de Partículas, Lisboa, Portugal
M. Araujo, P. Bargassa, D. Bastos, A. Boletti, P. Faccioli, M. Gallinaro, J. Hollar, N. Leonardo, T. Niknejad, M. Pisano, J. Seixas, O. Toldaiev, J. Varela

Joint Institute for Nuclear Research, Dubna, Russia
S. Afanasiev, D. Budkouski, I. Golutvin, I. Gorbunov, V. Karjavine, V. Korenkov, A. Lanev, A. Malakhov, V. Matveev[49,50], V. Palichik, V. Perelygin, M. Savina, D. Seitova, V. Shalaev, S. Shmatov, S. Shulha, V. Smirnov, O. Teryaev, N. Voytishin, B.S. Yuldashev[51], A. Zarubin, I. Zhizhin

Petersburg Nuclear Physics Institute, Gatchina (St. Petersburg), Russia
G. Gavrilov, V. Golovtcov, Y. Ivanov, V. Kim[52], E. Kuznetsova[53], V. Murzin, V. Oreshkin, I. Smirnov, D. Sosnov, V. Sulimov, L. Uvarov, S. Volkov, A. Vorobyev

Institute for Nuclear Research, Moscow, Russia
Yu. Andreev, A. Dermenev, S. Gninenko, N. Golubev, A. Karneyeu, D. Kirpichnikov, M. Kirsanov, N. Krasnikov, A. Pashenkov, G. Pivovarov, D. Tlisov[†], A. Toropin

Institute for Theoretical and Experimental Physics named by A.I. Alikhanov of NRC 'Kurchatov Institute', Moscow, Russia
V. Epshteyn, V. Gavrilov, N. Lychkovskaya, A. Nikitenko[54], V. Popov, A. Spiridonov, A. Stepennov, M. Toms, E. Vlasov, A. Zhokin

Moscow Institute of Physics and Technology, Moscow, Russia
T. Aushev

National Research Nuclear University 'Moscow Engineering Physics Institute' (MEPhI), Moscow, Russia
R. Chistov[55], M. Danilov[55], A. Oskin, P. Parygin, S. Polikarpov[55]

P.N. Lebedev Physical Institute, Moscow, Russia
V. Andreev, M. Azarkin, I. Dremin, M. Kirakosyan, A. Terkulov

Skobeltsyn Institute of Nuclear Physics, Lomonosov Moscow State University, Moscow, Russia
A. Belyaev, E. Boos, V. Bunichev, M. Dubinin[56], L. Dudko, A. Ershov, V. Klyukhin, N. Korneeva, I. Lokhtin, S. Obraztsov, M. Perfilov, V. Savrin, P. Volkov

Novosibirsk State University (NSU), Novosibirsk, Russia
V. Blinov[57], T. Dimova[57], L. Kardapoltsev[57], A. Kozyrev[57], I. Ovtin[57], Y. Skovpen[57]

Institute for High Energy Physics of National Research Centre 'Kurchatov Institute', Protvino, Russia
I. Azhgirey, I. Bayshev, D. Elumakhov, V. Kachanov, D. Konstantinov, P. Mandrik, V. Petrov, R. Ryutin, S. Slabospitskii, A. Sobol, S. Troshin, N. Tyurin, A. Uzunian, A. Volkov

National Research Tomsk Polytechnic University, Tomsk, Russia
A. Babaev, V. Okhotnikov

Tomsk State University, Tomsk, Russia
V. Borshch, V. Ivanchenko, E. Tcherniaev

University of Belgrade: Faculty of Physics and VINCA Institute of Nuclear Sciences, Belgrade, Serbia
P. Adzic[58], M. Dordevic, P. Milenovic, J. Milosevic

Centro de Investigaciones Energéticas Medioambientales y Tecnológicas (CIEMAT), Madrid, Spain
M. Aguilar-Benitez, J. Alcaraz Maestre, A. Álvarez Fernández, I. Bachiller, M. Barrio Luna, Cristina F. Bedoya, C.A. Carrillo Montoya, M. Cepeda, M. Cerrada, N. Colino, B. De La Cruz, A. Delgado Peris, J.P. Fernández Ramos, J. Flix, M.C. Fouz, O. Gonzalez Lopez, S. Goy Lopez, J.M. Hernandez, M.I. Josa, J. León Holgado, D. Moran, Á. Navarro Tobar, A. Pérez-Calero Yzquierdo, J. Puerta Pelayo, I. Redondo, L. Romero, S. Sánchez Navas, L. Urda Gómez, C. Willmott

Universidad Autónoma de Madrid, Madrid, Spain
J.F. de Trocóniz, R. Reyes-Almanza

Universidad de Oviedo, Instituto Universitario de Ciencias y Tecnologías Espaciales de Asturias (ICTEA), Oviedo, Spain
B. Alvarez Gonzalez, J. Cuevas, C. Erice, J. Fernandez Menendez, S. Folgueras, I. Gonzalez Caballero, J.R. González Fernández, E. Palencia Cortezon, C. Ramón Álvarez, J. Ripoll Sau, V. Rodríguez Bouza, A. Trapote, N. Trevisani

Instituto de Física de Cantabria (IFCA), CSIC-Universidad de Cantabria, Santander, Spain
J.A. Brochero Cifuentes, I.J. Cabrillo, A. Calderon, J. Duarte Campderros, M. Fernandez, C. Fernandez Madrazo, P.J. Fernández Manteca, A. García Alonso, G. Gomez, C. Martinez Rivero, P. Martinez Ruiz del Arbol, F. Matorras, P. Matorras Cuevas, J. Piedra Gomez, C. Prieels, T. Rodrigo, A. Ruiz-Jimeno, L. Scodellaro, I. Vila, J.M. Vizan Garcia

University of Colombo, Colombo, Sri Lanka
MK Jayananda, B. Kailasapathy[59], D.U.J. Sonnadara, DDC Wickramarathna

University of Ruhuna, Department of Physics, Matara, Sri Lanka
W.G.D. Dharmaratna, K. Liyanage, N. Perera, N. Wickramage

CERN, European Organization for Nuclear Research, Geneva, Switzerland
T.K. Aarrestad, D. Abbaneo, J. Alimena, E. Auffray, G. Auzinger, J. Baechler, P. Baillon[†], D. Barney, J. Bendavid, M. Bianco, A. Bocci, T. Camporesi, M. Capeans Garrido, G. Cerminara, S.S. Chhibra, M. Cipriani, L. Cristella, D. d'Enterria, A. Dabrowski, N. Daci, A. David, A. De Roeck, M.M. Defranchis, M. Deile, M. Dobson, M. Dünser, N. Dupont, A. Elliott-Peisert, N. Emriskova, F. Fallavollita[60], D. Fasanella, S. Fiorendi, A. Florent, G. Franzoni, W. Funk, S. Giani, D. Gigi, K. Gill, F. Glege, L. Gouskos, M. Haranko, J. Hegeman, Y. Iiyama, V. Innocente, T. James, P. Janot, J. Kaspar, J. Kieseler, M. Komm, N. Kratochwil, C. Lange, S. Laurila, P. Lecoq, K. Long, C. Lourenço, L. Malgeri, S. Mallios, M. Mannelli, A.C. Marini, F. Meijers, S. Mersi, E. Meschi, F. Moortgat, M. Mulders, S. Orfanelli, L. Orsini, F. Pantaleo, L. Pape, E. Perez, M. Peruzzi, A. Petrilli, G. Petrucciani, A. Pfeiffer, M. Pierini, D. Piparo, M. Pitt, H. Qu, T. Quast, D. Rabady, A. Racz, G. Reales Gutiérrez, M. Rieger, M. Rovere, H. Sakulin, J. Salfeld-Nebgen, S. Scarfi, C. Schäfer, C. Schwick, M. Selvaggi, A. Sharma, P. Silva, W. Snoeys, P. Sphicas[61], S. Summers, K. Tatar, V.R. Tavolaro, D. Treille, A. Tsirou, G.P. Van Onsem, M. Verzetti, J. Wanczyk[62], K.A. Wozniak, W.D. Zeuner

Paul Scherrer Institut, Villigen, Switzerland
L. Caminada[63], A. Ebrahimi, W. Erdmann, R. Horisberger, Q. Ingram, H.C. Kaestli, D. Kotlinski, U. Langenegger, M. Missiroli, T. Rohe

ETH Zurich - Institute for Particle Physics and Astrophysics (IPA), Zurich, Switzerland
K. Androsov[62], M. Backhaus, P. Berger, A. Calandri, N. Chernyavskaya, A. De Cosa, G. Dissertori, M. Dittmar, M. Donegà, C. Dorfer, F. Eble, K. Gedia, F. Glessgen, T.A. Gómez Espinosa, C. Grab, D. Hits, W. Lustermann, A.-M. Lyon, R.A. Manzoni, C. Martin Perez, M.T. Meinhard, F. Nessi-Tedaldi, J. Niedziela, F. Pauss, V. Perovic, S. Pigazzini, M.G. Ratti, M. Reichmann, C. Reissel, T. Reitenspiess, B. Ristic, D. Ruini, D.A. Sanz Becerra, M. Schönenberger, V. Stampf, J. Steggemann[62], R. Wallny, D.H. Zhu

Universität Zürich, Zurich, Switzerland
C. Amsler[64], P. Bärtschi, C. Botta, D. Brzhechko, M.F. Canelli, K. Cormier, A. De Wit, R. Del Burgo, J.K. Heikkilä, M. Huwiler, W. Jin, A. Jofrehei, B. Kilminster, S. Leontsinis, S.P. Liechti, A. Macchiolo, P. Meiring, V.M. Mikuni, U. Molinatti, I. Neutelings, A. Reimers, P. Robmann, S. Sanchez Cruz, K. Schweiger, Y. Takahashi

National Central University, Chung-Li, Taiwan
C. Adloff[65], C.M. Kuo, W. Lin, A. Roy, T. Sarkar[36], S.S. Yu

National Taiwan University (NTU), Taipei, Taiwan
L. Ceard, Y. Chao, K.F. Chen, P.H. Chen, W.-S. Hou, Y.y. Li, R.-S. Lu, E. Paganis, A. Psallidas, A. Steen, H.y. Wu, E. Yazgan, P.r. Yu

Chulalongkorn University, Faculty of Science, Department of Physics, Bangkok, Thailand
B. Asavapibhop, C. Asawatangtrakuldee, N. Srimanobhas

Çukurova University, Physics Department, Science and Art Faculty, Adana, Turkey
F. Boran, S. Damarseckin[66], Z.S. Demiroglu, F. Dolek, I. Dumanoglu[67], E. Eskut, Y. Guler, E. Gurpinar Guler[68], I. Hos[69], C. Isik, O. Kara, A. Kayis Topaksu, U. Kiminsu, G. Onengut, K. Ozdemir[70], A. Polatoz, A.E. Simsek, B. Tali[71], U.G. Tok, S. Turkcapar, I.S. Zorbakir, C. Zorbilmez

Middle East Technical University, Physics Department, Ankara, Turkey
B. Isildak[72], G. Karapinar[73], K. Ocalan[74], M. Yalvac[75]

Bogazici University, Istanbul, Turkey
B. Akgun, I.O. Atakisi, E. Gülmez, M. Kaya[76], O. Kaya[77], Ö. Özçelik, S. Tekten[78], E.A. Yetkin[79]

Istanbul Technical University, Istanbul, Turkey
A. Cakir, K. Cankocak[67], Y. Komurcu, S. Sen[80]

Istanbul University, Istanbul, Turkey
S. Cerci[71], B. Kaynak, S. Ozkorucuklu, D. Sunar Cerci[71]

Institute for Scintillation Materials of National Academy of Science of Ukraine, Kharkov, Ukraine
B. Grynyov

National Scientific Center, Kharkov Institute of Physics and Technology, Kharkov, Ukraine
L. Levchuk

University of Bristol, Bristol, United Kingdom
D. Anthony, E. Bhal, S. Bologna, J.J. Brooke, A. Bundock, E. Clement, D. Cussans, H. Flacher, J. Goldstein, G.P. Heath, H.F. Heath, M.l. Holmberg[81], L. Kreczko, B. Krikler, S. Paramesvaran, S. Seif El Nasr-Storey, V.J. Smith, N. Stylianou[82], K. Walkingshaw Pass, R. White

Rutherford Appleton Laboratory, Didcot, United Kingdom
K.W. Bell, A. Belyaev[83], C. Brew, R.M. Brown, D.J.A. Cockerill, C. Cooke, K.V. Ellis, K. Harder,

S. Harper, J. Linacre, K. Manolopoulos, D.M. Newbold, E. Olaiya, D. Petyt, T. Reis, T. Schuh, C.H. Shepherd-Themistocleous, I.R. Tomalin, T. Williams

Imperial College, London, United Kingdom
R. Bainbridge, P. Bloch, S. Bonomally, J. Borg, S. Breeze, O. Buchmuller, V. Cepaitis, G.S. Chahal[84], D. Colling, P. Dauncey, G. Davies, M. Della Negra, S. Fayer, G. Fedi, G. Hall, M.H. Hassanshahi, G. Iles, J. Langford, L. Lyons, A.-M. Magnan, S. Malik, A. Martelli, D.G. Monk, J. Nash[85], M. Pesaresi, D.M. Raymond, A. Richards, A. Rose, E. Scott, C. Seez, A. Shtipliyski, A. Tapper, K. Uchida, T. Virdee[19], M. Vojinovic, N. Wardle, S.N. Webb, D. Winterbottom, A.G. Zecchinelli

Brunel University, Uxbridge, United Kingdom
K. Coldham, J.E. Cole, A. Khan, P. Kyberd, I.D. Reid, L. Teodorescu, S. Zahid

Baylor University, Waco, USA
S. Abdullin, A. Brinkerhoff, B. Caraway, J. Dittmann, K. Hatakeyama, A.R. Kanuganti, B. McMaster, N. Pastika, M. Saunders, S. Sawant, C. Sutantawibul, J. Wilson

Catholic University of America, Washington, DC, USA
R. Bartek, A. Dominguez, R. Uniyal, A.M. Vargas Hernandez

The University of Alabama, Tuscaloosa, USA
A. Buccilli, S.I. Cooper, D. Di Croce, S.V. Gleyzer, C. Henderson, C.U. Perez, P. Rumerio[86], C. West

Boston University, Boston, USA
A. Akpinar, A. Albert, D. Arcaro, C. Cosby, Z. Demiragli, E. Fontanesi, D. Gastler, J. Rohlf, K. Salyer, D. Sperka, D. Spitzbart, I. Suarez, A. Tsatsos, S. Yuan, D. Zou

Brown University, Providence, USA
G. Benelli, B. Burkle, X. Coubez[20], D. Cutts, M. Hadley, U. Heintz, J.M. Hogan[87], G. Landsberg, K.T. Lau, M. Lukasik, J. Luo, M. Narain, S. Sagir[88], E. Usai, W.Y. Wong, X. Yan, D. Yu, W. Zhang

University of California, Davis, Davis, USA
J. Bonilla, C. Brainerd, R. Breedon, M. Calderon De La Barca Sanchez, M. Chertok, J. Conway, P.T. Cox, R. Erbacher, G. Haza, F. Jensen, O. Kukral, R. Lander, M. Mulhearn, D. Pellett, B. Regnery, D. Taylor, Y. Yao, F. Zhang

University of California, Los Angeles, USA
M. Bachtis, R. Cousins, A. Datta, D. Hamilton, J. Hauser, M. Ignatenko, M.A. Iqbal, T. Lam, W.A. Nash, S. Regnard, D. Saltzberg, B. Stone, V. Valuev

University of California, Riverside, Riverside, USA
K. Burt, Y. Chen, R. Clare, J.W. Gary, M. Gordon, G. Hanson, G. Karapostoli, O.R. Long, N. Manganelli, M. Olmedo Negrete, W. Si, S. Wimpenny, Y. Zhang

University of California, San Diego, La Jolla, USA
J.G. Branson, P. Chang, S. Cittolin, S. Cooperstein, N. Deelen, D. Diaz, J. Duarte, R. Gerosa, L. Giannini, D. Gilbert, J. Guiang, R. Kansal, V. Krutelyov, R. Lee, J. Letts, M. Masciovecchio, S. May, M. Pieri, B.V. Sathia Narayanan, V. Sharma, M. Tadel, A. Vartak, F. Würthwein, Y. Xiang, A. Yagil

University of California, Santa Barbara - Department of Physics, Santa Barbara, USA
N. Amin, C. Campagnari, M. Citron, A. Dorsett, V. Dutta, J. Incandela, M. Kilpatrick, J. Kim, B. Marsh, H. Mei, M. Oshiro, M. Quinnan, J. Richman, U. Sarica, J. Sheplock, D. Stuart, S. Wang

California Institute of Technology, Pasadena, USA
A. Bornheim, O. Cerri, I. Dutta, J.M. Lawhorn, N. Lu, J. Mao, H.B. Newman, T.Q. Nguyen, M. Spiropulu, J.R. Vlimant, C. Wang, S. Xie, Z. Zhang, R.Y. Zhu

Carnegie Mellon University, Pittsburgh, USA
J. Alison, S. An, M.B. Andrews, P. Bryant, T. Ferguson, A. Harilal, C. Liu, T. Mudholkar, M. Paulini, A. Sanchez

University of Colorado Boulder, Boulder, USA
J.P. Cumalat, W.T. Ford, A. Hassani, E. MacDonald, R. Patel, A. Perloff, C. Savard, K. Stenson, K.A. Ulmer, S.R. Wagner

Cornell University, Ithaca, USA
J. Alexander, S. Bright-thonney, Y. Cheng, D.J. Cranshaw, S. Hogan, J. Monroy, J.R. Patterson, D. Quach, J. Reichert, M. Reid, A. Ryd, W. Sun, J. Thom, P. Wittich, R. Zou

Fermi National Accelerator Laboratory, Batavia, USA
M. Albrow, M. Alyari, G. Apollinari, A. Apresyan, A. Apyan, S. Banerjee, L.A.T. Bauerdick, D. Berry, J. Berryhill, P.C. Bhat, K. Burkett, J.N. Butler, A. Canepa, G.B. Cerati, H.W.K. Cheung, F. Chlebana, M. Cremonesi, K.F. Di Petrillo, V.D. Elvira, Y. Feng, J. Freeman, Z. Gecse, L. Gray, D. Green, S. Grünendahl, O. Gutsche, R.M. Harris, R. Heller, T.C. Herwig, J. Hirschauer, B. Jayatilaka, S. Jindariani, M. Johnson, U. Joshi, T. Klijnsma, B. Klima, K.H.M. Kwok, S. Lammel, D. Lincoln, R. Lipton, T. Liu, C. Madrid, K. Maeshima, C. Mantilla, D. Mason, P. McBride, P. Merkel, S. Mrenna, S. Nahn, J. Ngadiuba, V. O'Dell, V. Papadimitriou, K. Pedro, C. Pena[56], O. Prokofyev, F. Ravera, A. Reinsvold Hall, L. Ristori, B. Schneider, E. Sexton-Kennedy, N. Smith, A. Soha, W.J. Spalding, L. Spiegel, S. Stoynev, J. Strait, L. Taylor, S. Tkaczyk, N.V. Tran, L. Uplegger, E.W. Vaandering, H.A. Weber

University of Florida, Gainesville, USA
D. Acosta, P. Avery, D. Bourilkov, L. Cadamuro, V. Cherepanov, F. Errico, R.D. Field, D. Guerrero, B.M. Joshi, M. Kim, E. Koenig, J. Konigsberg, A. Korytov, K.H. Lo, K. Matchev, N. Menendez, G. Mitselmakher, A. Muthirakalayil Madhu, N. Rawal, D. Rosenzweig, S. Rosenzweig, K. Shi, J. Sturdy, J. Wang, E. Yigitbasi, X. Zuo

Florida State University, Tallahassee, USA
T. Adams, A. Askew, R. Habibullah, V. Hagopian, K.F. Johnson, R. Khurana, T. Kolberg, G. Martinez, H. Prosper, C. Schiber, O. Viazlo, R. Yohay, J. Zhang

Florida Institute of Technology, Melbourne, USA
M.M. Baarmand, S. Butalla, T. Elkafrawy[15], M. Hohlmann, R. Kumar Verma, D. Noonan, M. Rahmani, F. Yumiceva

University of Illinois at Chicago (UIC), Chicago, USA
M.R. Adams, H. Becerril Gonzalez, R. Cavanaugh, X. Chen, S. Dittmer, O. Evdokimov, C.E. Gerber, D.A. Hangal, D.J. Hofman, A.H. Merrit, C. Mills, G. Oh, T. Roy, S. Rudrabhatla, M.B. Tonjes, N. Varelas, J. Viinikainen, X. Wang, Z. Wu, Z. Ye

The University of Iowa, Iowa City, USA
M. Alhusseini, K. Dilsiz[89], R.P. Gandrajula, O.K. Köseyan, J.-P. Merlo, A. Mestvirishvili[90], J. Nachtman, H. Ogul[91], Y. Onel, A. Penzo, C. Snyder, E. Tiras[92]

Johns Hopkins University, Baltimore, USA
O. Amram, B. Blumenfeld, L. Corcodilos, J. Davis, M. Eminizer, A.V. Gritsan, S. Kyriacou, P. Maksimovic, J. Roskes, M. Swartz, T.Á. Vámi

The University of Kansas, Lawrence, USA
A. Abreu, J. Anguiano, C. Baldenegro Barrera, P. Baringer, A. Bean, A. Bylinkin, Z. Flowers, T. Isidori, S. Khalil, J. King, G. Krintiras, A. Kropivnitskaya, M. Lazarovits, C. Lindsey, J. Marquez, N. Minafra, M. Murray, M. Nickel, C. Rogan, C. Royon, R. Salvatico, S. Sanders, E. Schmitz, C. Smith, J.D. Tapia Takaki, Q. Wang, Z. Warner, J. Williams, G. Wilson

Kansas State University, Manhattan, USA
S. Duric, A. Ivanov, K. Kaadze, D. Kim, Y. Maravin, T. Mitchell, A. Modak, K. Nam

Lawrence Livermore National Laboratory, Livermore, USA
F. Rebassoo, D. Wright

University of Maryland, College Park, USA
E. Adams, A. Baden, O. Baron, A. Belloni, S.C. Eno, N.J. Hadley, S. Jabeen, R.G. Kellogg, T. Koeth, A.C. Mignerey, S. Nabili, C. Palmer, M. Seidel, A. Skuja, L. Wang, K. Wong

Massachusetts Institute of Technology, Cambridge, USA
D. Abercrombie, G. Andreassi, R. Bi, S. Brandt, W. Busza, I.A. Cali, Y. Chen, M. D'Alfonso, J. Eysermans, C. Freer, G. Gomez Ceballos, M. Goncharov, P. Harris, M. Hu, M. Klute, D. Kovalskyi, J. Krupa, Y.-J. Lee, B. Maier, C. Mironov, C. Paus, D. Rankin, C. Roland, G. Roland, Z. Shi, G.S.F. Stephans, J. Wang, Z. Wang, B. Wyslouch

University of Minnesota, Minneapolis, USA
R.M. Chatterjee, A. Evans, P. Hansen, J. Hiltbrand, Sh. Jain, M. Krohn, Y. Kubota, J. Mans, M. Revering, R. Rusack, R. Saradhy, N. Schroeder, N. Strobbe, M.A. Wadud

University of Nebraska-Lincoln, Lincoln, USA
K. Bloom, M. Bryson, S. Chauhan, D.R. Claes, C. Fangmeier, L. Finco, F. Golf, C. Joo, I. Kravchenko, M. Musich, I. Reed, J.E. Siado, G.R. Snow[+], W. Tabb, F. Yan

State University of New York at Buffalo, Buffalo, USA
G. Agarwal, H. Bandyopadhyay, L. Hay, I. Iashvili, A. Kharchilava, C. McLean, D. Nguyen, J. Pekkanen, S. Rappoccio, A. Williams

Northeastern University, Boston, USA
G. Alverson, E. Barberis, Y. Haddad, A. Hortiangtham, J. Li, G. Madigan, B. Marzocchi, D.M. Morse, V. Nguyen, T. Orimoto, A. Parker, L. Skinnari, A. Tishelman-Charny, T. Wamorkar, B. Wang, A. Wisecarver, D. Wood

Northwestern University, Evanston, USA
S. Bhattacharya, J. Bueghly, Z. Chen, A. Gilbert, T. Gunter, K.A. Hahn, Y. Liu, N. Odell, M.H. Schmitt, M. Velasco

University of Notre Dame, Notre Dame, USA
R. Band, R. Bucci, A. Das, N. Dev, R. Goldouzian, M. Hildreth, K. Hurtado Anampa, C. Jessop, K. Lannon, J. Lawrence, N. Loukas, D. Lutton, N. Marinelli, I. Mcalister, T. McCauley, F. Meng, K. Mohrman, Y. Musienko[49], R. Ruchti, P. Siddireddy, A. Townsend, M. Wayne, A. Wightman, M. Wolf, M. Zarucki, L. Zygala

The Ohio State University, Columbus, USA
B. Bylsma, B. Cardwell, L.S. Durkin, B. Francis, C. Hill, M. Nunez Ornelas, K. Wei, B.L. Winer, B.R. Yates

Princeton University, Princeton, USA
F.M. Addesa, B. Bonham, P. Das, G. Dezoort, P. Elmer, A. Frankenthal, B. Greenberg,

N. Haubrich, S. Higginbotham, A. Kalogeropoulos, G. Kopp, S. Kwan, D. Lange, M.T. Lucchini, D. Marlow, K. Mei, I. Ojalvo, J. Olsen, D. Stickland, C. Tully

University of Puerto Rico, Mayaguez, USA
S. Malik, S. Norberg

Purdue University, West Lafayette, USA
A.S. Bakshi, V.E. Barnes, R. Chawla, S. Das, L. Gutay, M. Jones, A.W. Jung, S. Karmarkar, M. Liu, G. Negro, N. Neumeister, G. Paspalaki, C.C. Peng, S. Piperov, A. Purohit, J.F. Schulte, M. Stojanovic[16], J. Thieman, F. Wang, R. Xiao, W. Xie

Purdue University Northwest, Hammond, USA
J. Dolen, N. Parashar

Rice University, Houston, USA
A. Baty, M. Decaro, S. Dildick, K.M. Ecklund, S. Freed, P. Gardner, F.J.M. Geurts, A. Kumar, W. Li, B.P. Padley, R. Redjimi, W. Shi, A.G. Stahl Leiton, S. Yang, L. Zhang, Y. Zhang

University of Rochester, Rochester, USA
A. Bodek, P. de Barbaro, R. Demina, J.L. Dulemba, C. Fallon, T. Ferbel, M. Galanti, A. Garcia-Bellido, O. Hindrichs, A. Khukhunaishvili, E. Ranken, R. Taus

Rutgers, The State University of New Jersey, Piscataway, USA
B. Chiarito, J.P. Chou, A. Gandrakota, Y. Gershtein, E. Halkiadakis, A. Hart, M. Heindl, O. Karacheban[23], I. Laflotte, A. Lath, R. Montalvo, K. Nash, M. Osherson, S. Salur, S. Schnetzer, S. Somalwar, R. Stone, S.A. Thayil, S. Thomas, H. Wang

University of Tennessee, Knoxville, USA
H. Acharya, A.G. Delannoy, S. Spanier

Texas A&M University, College Station, USA
O. Bouhali[93], M. Dalchenko, A. Delgado, R. Eusebi, J. Gilmore, T. Huang, T. Kamon[94], H. Kim, S. Luo, S. Malhotra, R. Mueller, D. Overton, D. Rathjens, A. Safonov

Texas Tech University, Lubbock, USA
N. Akchurin, J. Damgov, V. Hegde, S. Kunori, K. Lamichhane, S.W. Lee, T. Mengke, S. Muthumuni, T. Peltola, I. Volobouev, Z. Wang, A. Whitbeck

Vanderbilt University, Nashville, USA
E. Appelt, S. Greene, A. Gurrola, W. Johns, A. Melo, H. Ni, K. Padeken, F. Romeo, P. Sheldon, S. Tuo, J. Velkovska

University of Virginia, Charlottesville, USA
M.W. Arenton, B. Cox, G. Cummings, J. Hakala, R. Hirosky, M. Joyce, A. Ledovskoy, A. Li, C. Neu, B. Tannenwald, S. White, E. Wolfe

Wayne State University, Detroit, USA
N. Poudyal

University of Wisconsin - Madison, Madison, WI, USA
K. Black, T. Bose, J. Buchanan, C. Caillol, S. Dasu, I. De Bruyn, P. Everaerts, F. Fienga, C. Galloni, H. He, M. Herndon, A. Hervé, U. Hussain, A. Lanaro, A. Loeliger, R. Loveless, J. Madhusudanan Sreekala, A. Mallampalli, A. Mohammadi, D. Pinna, A. Savin, V. Shang, V. Sharma, W.H. Smith, D. Teague, S. Trembath-reichert, W. Vetens

†: Deceased

1: Also at TU Wien, Wien, Austria

2: Also at Institute of Basic and Applied Sciences, Faculty of Engineering, Arab Academy for Science, Technology and Maritime Transport, Alexandria, Egypt, Alexandria, Egypt

3: Also at Université Libre de Bruxelles, Bruxelles, Belgium

4: Also at Universidade Estadual de Campinas, Campinas, Brazil

5: Also at Federal University of Rio Grande do Sul, Porto Alegre, Brazil

6: Also at University of Chinese Academy of Sciences, Beijing, China

7: Also at Department of Physics, Tsinghua University, Beijing, China, Beijing, China

8: Also at UFMS, Nova Andradina, Brazil

9: Also at Nanjing Normal University Department of Physics, Nanjing, China

10: Now at The University of Iowa, Iowa City, USA

11: Also at Institute for Theoretical and Experimental Physics named by A.I. Alikhanov of NRC 'Kurchatov Institute', Moscow, Russia

12: Also at Joint Institute for Nuclear Research, Dubna, Russia

13: Also at Cairo University, Cairo, Egypt

14: Also at British University in Egypt, Cairo, Egypt

15: Now at Ain Shams University, Cairo, Egypt

16: Also at Purdue University, West Lafayette, USA

17: Also at Université de Haute Alsace, Mulhouse, France

18: Also at Erzincan Binali Yildirim University, Erzincan, Turkey

19: Also at CERN, European Organization for Nuclear Research, Geneva, Switzerland

20: Also at RWTH Aachen University, III. Physikalisches Institut A, Aachen, Germany

21: Also at University of Hamburg, Hamburg, Germany

22: Also at Department of Physics, Isfahan University of Technology, Isfahan, Iran, Isfahan, Iran

23: Also at Brandenburg University of Technology, Cottbus, Germany

24: Also at Skobeltsyn Institute of Nuclear Physics, Lomonosov Moscow State University, Moscow, Russia

25: Also at Physics Department, Faculty of Science, Assiut University, Assiut, Egypt

26: Also at Karoly Robert Campus, MATE Institute of Technology, Gyongyos, Hungary

27: Also at Institute of Physics, University of Debrecen, Debrecen, Hungary, Debrecen, Hungary

28: Also at Institute of Nuclear Research ATOMKI, Debrecen, Hungary

29: Also at MTA-ELTE Lendület CMS Particle and Nuclear Physics Group, Eötvös Loránd University, Budapest, Hungary, Budapest, Hungary

30: Also at Wigner Research Centre for Physics, Budapest, Hungary

31: Also at IIT Bhubaneswar, Bhubaneswar, India, Bhubaneswar, India

32: Also at Institute of Physics, Bhubaneswar, India

33: Also at G.H.G. Khalsa College, Punjab, India

34: Also at Shoolini University, Solan, India

35: Also at University of Hyderabad, Hyderabad, India

36: Also at University of Visva-Bharati, Santiniketan, India

37: Also at Indian Institute of Technology (IIT), Mumbai, India

38: Also at Deutsches Elektronen-Synchrotron, Hamburg, Germany

39: Also at Sharif University of Technology, Tehran, Iran

40: Also at Department of Physics, University of Science and Technology of Mazandaran, Behshahr, Iran

41: Now at INFN Sezione di Bari [a], Università di Bari [b], Politecnico di Bari [c], Bari, Italy

42: Also at Italian National Agency for New Technologies, Energy and Sustainable Economic Development, Bologna, Italy

43: Also at Centro Siciliano di Fisica Nucleare e di Struttura Della Materia, Catania, Italy

44: Also at Università di Napoli 'Federico II', NAPOLI, Italy

45: Also at Consiglio Nazionale delle Ricerche - Istituto Officina dei Materiali, PERUGIA, Italy

46: Also at Riga Technical University, Riga, Latvia, Riga, Latvia

47: Also at Consejo Nacional de Ciencia y Tecnología, Mexico City, Mexico

48: Also at IRFU, CEA, Université Paris-Saclay, Gif-sur-Yvette, France

49: Also at Institute for Nuclear Research, Moscow, Russia

50: Now at National Research Nuclear University 'Moscow Engineering Physics Institute' (MEPhI), Moscow, Russia

51: Also at Institute of Nuclear Physics of the Uzbekistan Academy of Sciences, Tashkent, Uzbekistan

52: Also at St. Petersburg State Polytechnical University, St. Petersburg, Russia

53: Also at University of Florida, Gainesville, USA

54: Also at Imperial College, London, United Kingdom

55: Also at P.N. Lebedev Physical Institute, Moscow, Russia

56: Also at California Institute of Technology, Pasadena, USA

57: Also at Budker Institute of Nuclear Physics, Novosibirsk, Russia

58: Also at Faculty of Physics, University of Belgrade, Belgrade, Serbia

59: Also at Trincomalee Campus, Eastern University, Sri Lanka, Nilaveli, Sri Lanka

60: Also at INFN Sezione di Pavia [a], Università di Pavia [b], Pavia, Italy, Pavia, Italy

61: Also at National and Kapodistrian University of Athens, Athens, Greece

62: Also at Ecole Polytechnique Fédérale Lausanne, Lausanne, Switzerland

63: Also at Universität Zürich, Zurich, Switzerland

64: Also at Stefan Meyer Institute for Subatomic Physics, Vienna, Austria, Vienna, Austria

65: Also at Laboratoire d'Annecy-le-Vieux de Physique des Particules, IN2P3-CNRS, Annecy-le-Vieux, France

66: Also at Şırnak University, Sirnak, Turkey

67: Also at Near East University, Research Center of Experimental Health Science, Nicosia, Turkey

68: Also at Konya Technical University, Konya, Turkey

69: Also at Istanbul University - Cerrahpasa, Faculty of Engineering, Istanbul, Turkey

70: Also at Piri Reis University, Istanbul, Turkey

71: Also at Adiyaman University, Adiyaman, Turkey

72: Also at Ozyegin University, Istanbul, Turkey

73: Also at Izmir Institute of Technology, Izmir, Turkey

74: Also at Necmettin Erbakan University, Konya, Turkey

75: Also at Bozok Universitetesi Rektörlügü, Yozgat, Turkey, Yozgat, Turkey

76: Also at Marmara University, Istanbul, Turkey

77: Also at Milli Savunma University, Istanbul, Turkey

78: Also at Kafkas University, Kars, Turkey

79: Also at Istanbul Bilgi University, Istanbul, Turkey

80: Also at Hacettepe University, Ankara, Turkey

81: Also at Rutherford Appleton Laboratory, Didcot, United Kingdom

82: Also at Vrije Universiteit Brussel, Brussel, Belgium

83: Also at School of Physics and Astronomy, University of Southampton, Southampton, United Kingdom

84: Also at IPPP Durham University, Durham, United Kingdom